Influence of the Biosphere on Precipitation: July 1995 studies with the ARM-CART Data

Y. C. Sud and D. M. Mocko* and G. K. Walker* and Randal D. Koster

Climate and Radiation Branch
Laboratory for Atmospheres
NASA/GSFC Greenbelt, MD 20771

Submitted to the Journal of Climate

Influence of the Biosphere on Precipitation: July 1995 study with the ARM-CART Data

Y. C. Sud and D. M. Mocko* and G. K. Walker* and Randal D. Koster

Climate and Radiation Branch
Laboratory for Atmospheres
NASA/GSFC Greenbelt, MD 20771

ABSTRACT

Ensemble sets of simulation experiments were conducted with a single column model (SCM) using the Goddard GEOS II GCM physics containing a recent version of the Cumulus Scheme (McRAS) and a biosphere based land-fluxes scheme (SSiB). The study used the 18 July to 5 August 1995 ARM-CART (Atmospheric Radiation Measurement-Cloud Atmospheric Radiation Test-bed) data, which was collected at the ARM-CART site in the mid-western United States and analyzed for single column modeling (SCM) studies. The new findings affirm the earlier findings that the vegetation, which increases the solar energy absorption at the surface together with soil and soil-moisture dependent processes, which modulate the surface, fluxes (particularly evapotranspiration) together help to increase the local rainfall. In addition, the results also show that for the particular study period roughly 50% of the increased evaporation over the ARM-CART site would be converted into rainfall with the Column, while the remainder would be advected out to the large-scale. Notwithstanding the limitations of only one-way interaction (i.e., the large-scale influencing the regional physics and not vice versa), the current SCM simulations show a very robust relationship. The evaporation-precipitation relationship turns out to be independent of the soil types, and soil moisture; however, it is weakly dependent on the vegetation cover because of its surface-albedo effect. Clearly, these inferences are prone to weaknesses of the SCM physics, the assumptions of the large-scale being unaffected by grid-scale (SCM-scale) changes in moist processes, and other limitations of the evaluation procedures.

1. Introduction

Earth's biosphere can influence fluxes in land-atmosphere interaction through four primary controls, namely by: (i) increased absorption of solar radiation within leaf organizations of vegetation canopies; (ii) increased evapotranspiration with access to root-zone soil moisture; (iii) stomatal control that generally stifles evapotranspiration during warm and/or dry episodes; and (iv) contributing surface roughness on the scale of turbulent eddies, which in turn increase the boundary layer depth and cross-isobaric moisture convergence in a typical surface-low pressure episode. In dry regions with small evapotranspiration, an increase in the surface-albedo reduces the solar absorption, land-surface fluxes, and rainfall (e.g., Sud and Molod, 1988; Dirmeyer and Shukla, 1994). Likewise, reduction of evapotranspiration and/or land-surface roughness -- a potential effect of removal of vegetation -- also decreases rainfall (e.g., Sud and Smith, 1985). In fact, a discernible dependence of rainfall on vegetation has been simulated and/or discussed in several papers (e.g., Dickinson, 1980; Anthes, 1984; Avissar, 1992; Sud and Fennessy, 1982, 1984). Moreover, the dependence of summer season precipitation on biospheric processes can be inferred from the first principles of moist-convection as enunciated by Arakawa and Schubert (1974). The very same principles have been used in the design of a whole generation of physically-based cumulus schemes, including RAS (Moorthi and Suarez, 1992), and McRAS (Sud and Walker, 1999). Sud et al. (1993, 1995) pedagogically argued and demonstrated that each vegetation process, when limited to influence only the column-atmosphere, helps to promote moist convection. Specifically, a surface albedo increase leads to near-surface energy deficit, reduces CAPE (Convective Available Potential Energy), and suppresses moist convection. On the other hand, simulations with altered proportions of evapotranspiration and sensible fluxes, for scenarios in which the sum of the surface fluxes remains invariant, reveal that evapotranspiration is a more desirable surface-flux for promoting convective rainfall because it enables CAPE-accumulation before "turning on" the moist-convection. Larger CAPE naturally enables convection to reach deeper into the atmosphere thereby producing

more precipitation and associated atmospheric warming. Since convective (as opposed to stratiform precipitation) produces less fractional cloud-cover, it naturally allows more insolation to reach the surface of the Earth, which further boosts the energy needed for surface fluxes. Together with the observational analyses (e.g., Otterman et al., 1990; Nicholson, 1985; and Skole and Tucker, 1993), such findings provide a rational physical basis for understanding the influence of vegetation on precipitation.

Even in several earlier studies, a warmer and drier climate was simulated in response to Amazonian deforestation (e.g., Dickinson and Henderson-Sellers, 1988; and Henderson-Sellers et al., 1993), even though there were significant differences in the simulated rainfall. The outcome became more perplexing when results of several GCMs (each with its own interactive biosphere) were examined side-by-side. Table 1 of Hahmann and Dickinson (1997) contains a comparison of evapotranspiration, moisture convergence, and local rainfall simulated by fifteen different GCMs used for simulating the influence of Amazonian deforestation. Even though a majority of models simulated a substantial decrease in rainfall in response to deforestation, a few models simulated an increase. This was caused by the competing effects of moisture convergence produced by the thermal heating of the lower troposphere vis-a-vis the moisture deficit produced by reduced evapotranspiration in deforestation (Eltahir and Bras, 1993). Recognizing that some differences in the Hahmann and Dickinson (1997) comparison would be due to differences in the location and the extent of the imposed deforestation anomalies or in the simulated climatic index of dryness (Koster and Suarez, 1999), it is also abundantly clear that the simulated findings continues to be model-dependent. Since models naturally simulate the synthesized outcome of modelled interactions between physics and dynamics, such variations in results point to the lack of satisfactory representation of modelled processes and their interaction with dynamics. We submit that there is a fundamental need for: (i) more extensive validation of modelled processes in GCMs; and (ii) devising more ingenious ways of examining the land-atmosphere interaction problem to arrive at a better answer. Consequently, we begin by examining the evidence of our model's

performance in a Single Column Model (SCM) using the prescribed large-scale forcing. Only after the evaluation are judged to be satisfactory, will we use the SCM to analyze its response to biosphere-precipitation interactions?

We examine the influence of the biosphere on the summer precipitation over the ARM-CART site of the mid-western Great Plains (for site details, see Randall and Cripe, 1999 Fig. 1, page 24,531). This region is affected by strong moisture advection by the low-level jet, which is a manifestation of the large-scale forcing. Our Single Column Model (SCM) of the atmosphere is coupled with simple SiB (SSiB) for simulating biosphere-atmosphere interactions that in turn are coupled to a highly resolved 1-D soil hydrology model that will be shown to yield a very accurate solution of Richard's equation. A state-of-the-art cloud scheme, called McRAS (Sud and Walker, 1999), is already coupled to the GEOS II GCM physics and has been shown to produce realistic results. The goal is to simulate most realistic soil-vegetation-atmosphere interactions, with the lower boundary condition at 5m below (water table may be higher) the surface of the soil. Assuming that such a model is realistic for the Great Plains region, what can we learn about the behavior of the column atmosphere to changes in surface fluxes? The question we pose is: if the large-scale atmosphere was essentially unaffected by much smaller-scale changes in the land-surface fluxes due to changes in vegetation cover or soil type or soil moisture, how would the vegetation-soil-rainfall interaction be affected locally? To examine this, we force the SCM to interact with a suite of soil types, soil moistures, and/or vegetation covers fractions. The July 1995 ARM-CART data represents wet conditions and we only perturb it towards drier conditions. We will describe our SCM, the cloud scheme called McRAS, and the new 100-layer soil-hydrology model in section 2. We also show concrete evidence of the intrinsic reliability of the SCM's physics and make a case for the suitability of this model for the proposed investigation in section 3. We then show key results of SCM studies with each of the five soil types adopted in the ISLSCP Initiative I data with a full range of soil moisture and vegetation covers in section

4. Finally we will discuss the implication of the findings for ecosystem and biosphere managers in section 5.

2. Single Column Model

Single column models (SCMs) have a long history of use for evaluating numerical models representing boundary-layer processes (e.g., Hoffert and Sud, 1976), land surface hydrology (Koster and Eagleson, 1990) and moist processes including convection and downdrafts (e.g., Cheng, 1989). Randall et al. (1996) discussed a variety of innovative uses of SCMs and illustrated how a single column model (SCM) would be a useful device for model parameterization evaluation and/or scientific hypothesis validation. We will use our SCM to validate the hypothesis that land-surface biospheric processes, particularly evapotranspiration, have a positive feedback effect on convective precipitation. To meet these goals, we force the SCM with observational data. This enables the investigator to differentiate between the mathematical and/or numerical characteristics of a particular parameterization vis-a-vis the model-simulated reality of the atmosphere. Our earlier results were that all biospheric processes help to promote the local rainfall, particularly the convective type everywhere, and that the inference is expected to hold for the mid-western United States typified by the ARM-CART site. However, the magnitude of this feedback was not discerned in those studies (sud et al., 1993).

The particular SCM is extensively described in Sud and Walker (1993) who used it for evaluating convective downdrafts using GATE Phase III data. More recently, Sud and Walker (1999) used the same SCM for evaluating the performance of a new Cloud microphysics with Relaxed Arakawa-Schubert Scheme (McRAS). The ARM-CART data is a new dataset for SCM use. Recently, it was analyzed and used for evaluating as well as model intercomparison of mid-latitude cloud processes (Ghan et al., 2000). Randall and Cripe (1999) discuss three different ways in which an SCM can be used for testing physical parameterizations. In the very basic form, i.e., without flux adjustments or artificial relaxation, which the authors call "Revealed Forcing", the specific humidity, q, tendency of the column atmosphere can be expressed by:

$$\frac{\partial q}{\partial t} = -\left[\nabla \bullet Vq + \frac{\partial \omega q}{\partial p}\right] + P. \qquad (1)$$

Here $\nabla \bullet Vq$ is the domain-averaged horizontal, and $\frac{\partial \omega q}{\partial p}$ is the domain-averaged vertical, flux divergence tendencies of q. Clearly, these tendencies are in the flux form and contain the sum of advective plus divergence tendencies. All the modelled physical processes are contained in the P-tendency, the last term of RHS. Equation (1) can be recast with the specific humidity q split three ways- (i) into observed, q_{obs}, (ii) land-surface fluxes forced anomaly, q_{veg}, and (iii) SCM- errors forced effect, q_{me}, as follows:

$$q = q_{obs} + q_{veg} + q_{me}. \qquad (2)$$

On substitution, Equation (1) becomes:

$$\frac{\partial q}{\partial t} = -\left[\nabla \bullet Vq_{obs} + \frac{\partial \omega q_{obs}}{\partial p}\right] - \left[\nabla \bullet Vq_{veg} + \frac{\partial \omega q_{veg}}{\partial p}\right] - \left[\nabla \bullet Vq_{m\varepsilon} + \frac{\partial \omega q_{me}}{\partial p}\right] + P. \qquad (3a)$$

The observed tendency can now is transformed into the basic advective form, which merely alters the first term of RHS to give:

$$\frac{\partial q}{\partial t} = -\left[V \bullet \nabla q_{obs} + \omega \frac{\partial q_{obs}}{\partial p}\right] - \left[\nabla \bullet Vq_{veg} + \frac{\partial \omega q_{veg}}{\partial p}\right] - \left[\nabla \bullet Vq_{me} + \frac{\partial \omega q_{me}}{\partial p}\right] + P. \qquad (3b)$$

A simulation, with no vegetation or soil-type anomalies, will have only the first and third terms of (3b) contained in square brackets of RHS, plus its tendency due to physical adjustment, P_{cont}. The land-surface fluxes anomaly simulation will have all the three terms, but each with its own physical adjustment term, P_{veg}. By appropriately accounting for these terms, we can delineate the vegetation and/or soil anomaly influence on the ensuing precipitation.

First let us rewrite (3b) in the following form:

$$\frac{\partial q}{\partial t} = - [O A T] - \left[\nabla \bullet V q_{me} + \frac{\partial \omega q_{me}}{\partial p}\right] + P_{cont}, \qquad (4a)$$

$$\frac{\partial q}{\partial t} = - [O A T] - \left[\nabla \bullet V(q_{me} + q_{veg}) + \frac{\partial \omega (q_{me} + q_{veg})}{\partial p}\right] + P_{veg} + P_{cont}, \qquad (4b)$$

where [O A T] is the observed advective tendency. The control and the anomalous land-surface fluxes simulations can be performed with the SCM using observed advective tendencies from the ARM-CART observations that get modulated by the second term of the RHS, which comprises of model errors and vegetation plus soil-type anomaly influences. The model is assumed to be realistic, but the model errors can be reduced largely, if not entirely, very much the way GCM-errors are expected to do in producing anomaly minus control differences. This would happen precisely if the errors had a linear influence. By subtracting simulation (4a) from (4b) or by comparing them side-by-side, we can hope to infer vegetation-produced tendencies with resultant physical interaction effects that would appear in a GCM with full hydrodynamics. Our analysis technique is a modification of the artificial relaxation methodology of Randall and Cripe (1999), because the advective equations have been recast to delineate the influence of surface fluxes on the ensuing changes in the column-atmosphere.

The second term in the square brackets of equations (4 a & b) represents the horizontal and vertical advective tendencies that are specific to the control and vegetation and/or soil anomaly simulations. To estimate them, we use the grid-cell domain-averaged horizontal wind, V, and vertical pressure velocity, ω, from observations. Both of them are provided in the ARM-CART SCM data. Our mode of testing would be the "revealed forcing" mode of Randall and Cripe (1999) with aforestated corrections. The second term of (4a) contains the following:

$$\frac{\partial q_{hor}}{\partial t} = - \frac{V_{obs} \bullet \nabla (q_{mod} - q_{obs})}{\Delta x} - (q_{mod} - q_{obs}) \nabla \bullet V_{obs}, \qquad (5)$$

where ΔX is the horizontal-length scale of the domain, while V_{obs} is taken to be constant. Here q_{mod} generically refers to the modelled q, which is different from q_{obs} due to model errors and/or vegetation anomaly influences, as stated before.

The second part is for the vertical flux divergence of q, or potential temperature, Θ, as the case may be. For the moisture, its form is:

$$\frac{\partial q_{vert}}{\partial t} = - \frac{\Delta \omega_{obs} (q_{mod} - q_{obs})}{\Delta p}. \qquad (6)$$

Here ω_{obs} is a function of p and must be multiplied with q-anomaly to conserve the anomalous moisture flux in the entire column during vertical advection. If we run all the cases involving different vegetation covers and soil-types by invoking (5 & 6) with or without including vegetation/soil effects, the influence of vegetation and/or soil-type on the parameterized physical interactions and observed advective tendency of q will be revealed. Whenever q of the SCM is different from the observed, the q advected in the horizontal and vertical direction is adjusted. The formulae are conceptually similar to that of Randall and Cripe (1999), except that our horizontal time constant τ is simply:

$$\tau_{hor} = \text{Horizontal Grid-length scale/Horizontal wind velocity.} \qquad (7)$$

A parallel equation can be written for other tendencies of which potential temperature Θ is directly relevant. If the SCM's q or Θ are influenced by surface processes, there is an appropriate adjustment for all material quantities and conserved variables.

2.1 Cloud Model

The cloud model of our SCM is McRAS (Microphysics of clouds with Relaxed Arakawa-Schubert Scheme) and was designed and developed with the aim of simulating realistic moist processes, clouds, and cloud-radiation interactions in GCMs. McRAS distinguishes and parameterizes three types of clouds: convective, stratiform, and boundary layer as shown schematically in Figure 1. The Relaxed Arakawa-Schubert scheme (RAS) of Moorthi and Suarez (1992) generates

convective clouds, but the cloud-microphysics follows Sud and Walker (1999). The simulated convective clouds transform and merge into stratiform clouds on 1-h time-scale, while the boundary-layer clouds merge into the stratiform clouds instantly. The cloud condensate converts into precipitation following the auto-conversion equations of Sundqvist (1988, 1993) that contain a parametric adaptation for the Bergeron-Findeisen process of ice crystal growth and collection of cloud condensate by precipitation. All clouds convect, advect and diffuse vertically (but not horizontally in the SCM-mode of testing) with a fully interactive cloud-microphysics. In this way, the life cycle of the cloud is related to cloud dynamics and microphysics, while their optical properties are derived from the statistical distribution of hydrometeors and idealized geometry of clouds. An evaluation of McRAS in a Single Column Model (SCM) with the GATE Phase III data was given in Sud and Walker (1999). It showed that together with the rest of the model physics, McRAS simulates the observed temperature, humidity, and precipitation without discernible systematic errors. The time-history and time-mean incloud water and ice distribution, fractional cloudiness, cloud optical thickness, origin of precipitation in the convective anvils and towers, and the convective updraft and downdraft velocities and mass fluxes all simulate a realistic behavior, even though all the diagnostics were not verifiable from the available data.

In order to determine the suitability of McRAS for ARM-CART data use, McRAS was evaluated for with two ARM-CART datasets: CASE 1 and 3. The cloud scheme was run using data without the model error adjustments discussed above. The results are shown in Figs. 2a through 2c. Even though the model with GATE PHASE III data (Sud and Walker, 1999) was virtually error-free, we noted a few systematic errors in this evaluation. The SCM produced somewhat less rainfall than observed, and its lapse rate near the surface was very different from the one given in the data. For now, we must contend with the former because there are negligible column integrated humidity errors in these simulations, while the horizontal advective tendency, and the surface evaporation data were prescribed from observations. Therefore, any significant mismatch between the observed and SCM-simulated time mean rainfall reveals

a lack of moisture conservation in the forcing ARM-CART data because our SCM naturally employs an internally consistent moisture conserving schemes.

2.2 Land Model

Our basic land model is the Simple SiB (SSiB) due to Xue et al (1991). This model has been tested with several datasets, but due to factors discussed in the Section I, land models of the present-day need to be constantly evaluated and improved, even region by region. A brief discussion of these improvements can be found in Mocko and Sud (2000, in preparation). One also notices SSiB parameterizes inter-layer hydraulic conduction among its layers with Richard's Equation with several arbitrary assumptions, which, in a crude way, help to give reasonable vertical fluxes. We felt there was a need to generate more accurate solutions of Richard's equation with better numerical rigor. Consequently, we solved the equation with much higher resolution. We finally settled on 100-layers model with 5cm resolution (Fig 3a). It is not suitable for GCM work but is useful for developing a parameterization of hydraulic conduction for land, which has no subgrid-scale variability. Indeed, lack of subgrid scale variability is an obvious limitation of the current SCM, but that is a separate issue and we reserve its treatment for a later time. Thus, the soil model has the bottom at 5m depth while the vegetation (root zone) layers of SSiB may vary regionally as a function of soil type and vegetation covers. SSiB was evaluated with ISLSCP Initiative I data under GSWP (Dirmeyer et al, 1999) as well as against other simple Land-Schemes (Mocko and Sud, 1998). The dataset covers a period of twenty-four months: January 1, 1987 through December 31, 1988. In this data, only five (Table 1, Fig. 3b) soil types were used to represent the entire world, while there could be 10 different biomes; nevertheless, any one grid cell could have only one soil type and one biome. In other words, tiling is not feasible in the SSiB design. The subgrid-scale variability is addressed by allowing full flexibility in choice of fractional vegetation cover and leaf area indices. The new 100-layer model was extensively tested with ISLSCP Initiative I data without use of any tuning factors for a range of conditions-from extremely dry to highly moist. The model is able to generate realistic soil-

water transport time-scales for all soil types and plausible vegetation processes.

As an example, we show in Fig. 4a how altering the vegetation in the ARM-CART site from a desert to a fully vegetated ground cover would affect the soil moisture and land-hydrology. Desert conditions lead to less evaporation and higher soil moisture and soil water drainage or runoff, while full vegetation cover produces more evaporation and less soil moisture and runoff. These differences are clearly noted in the difference maps (Fig 4b). Such evaluations were made for monsoonal India, Sahel, Mississippi basin, and over a dozen other regions of the world (not shown). All these regions simulated very realistic behaviors. Without the aid of vegetation to remove the soil-water by transpiration, the soil moisture fraction in the month of June at 1-1.5 m depth can become as high as 0.6 versus 0.3 for the simulation with natural vegetation cover (top Panel, Fig. 4b). With 99% vegetation cover, there is a systematic reduction of soil moisture, particularly in the spring season in which there is considerable soil moisture uptake by transpiration. However, in late summer, the soil moisture does not go much below its value for the natural ground cover because vegetation starts to wilt in the dry periods. Similar results are noted for Sahel, which has an extended dry period (Fig. 5a & b). In fact, with the onset of the rainy season, the soil wetting time for the deep soil is of the order of 10-20 days as can be noted from the slope of the soil moisture isohalines going into the deeper regions of the soil. Once wetted, the adjustment time scale is much smaller. Regardless, wetter (drier) soil up to 3m depth is noted for minimal (maximal) vegetation cover simulations. Having satisfied ourselves of a reasonably realistic performance of the hydraulic model, we linked the 100-layer soil-SSiB model to the atmospheric SCM to conduct the vegetation-soil-atmospheric interaction studies.

3. Design of the Experiment.

The SCM (Sud and Walker, 1993 & 1999) with GEOS II GCM physics and McRAS now has a 100-layer soil model (Koster et al., 2000), which hydrologically responds to the natural

vegetation in SSiB. To evaluate the influence of vegetation on the rainfall in the mid-western region, we employ ARM-CART data for Case 1. This is a 3-week dataset: July 18, 1995 through August 5, 1995, averaged over a 300x300 Km region in Kansas and Oklahoma (called ARM-CART site). Even though the ISLSCP Initiative I data indicates roughly 60% vegetation cover, we allowed the vegetation cover to vary from 1% to 99% in this investigation. This helped to delineate the influence of vegetation on the simulated rainfall. Our experiment is the SCM equivalent of a regional experiment in which the large-scale forcing is prescribed through Analysis of Observations, whereas the region is free to respond with changes in its surface fluxes, but with parameterizations attempting to represent the changes in meso-scale circulation. The influence of vegetation on surface fluxes and therefore the temperature and humidity will be communicated in the vertical through physical processes, namely turbulence, dry convection, and moisture-cloud-radiative forcing of the column atmosphere. Clearly, we also have the freedom to alter the soil type with a better-resolved calculation of soil-moisture dependent soil properties. Since ISLSCP Initiative I recommended 5 possible soil types for the world, and there is a possibility of large variations in soil types in a typical 300X300-km grid, we tested the SCM with each soil type using the same observed forcings. The initial soil moisture profile were obtained by making a long run with ISLSCP Initiative I data, and because of the differences in the hydraulic conduction properties of different soil to episodic rainfall events, the soil water profiles generated with different soils were so different in the structural complexity that we had to run each soil type and vegetation cover for six months prior to the simulation to get a reasonable estimate of the soil-moisture at the initial time. We ran a suite of 30 runs - one each for six values of fractional vegetation covers with each of the five soil-types. These are called control runs. The initial soil moisture profiles for each of the thirty cases are given in Fig. 6. We further produced an ensemble of five sets of thirty simulations each, in which the initial soil moisture profile of the 60% vegetation cover for each soil type was varied to introduce additional soil dryness 0%, 25%, 50%, 75% and 100% of soil moisture deficit = 1- f_s, where f_s is the soil moisture. These runs were used to analyze the relationships among soil-moisture, soil-type,

vegetation cover, and rainfall.

4. Results.

The objective of the current study is to determine the influence of vegetation on the rainfall in the mid-western United States. This test bed is a 300x300 Km region in Kansas and Oklahoma (called ARM-CART site). The site provides surface fluxes, top of the atmosphere radiative inputs, and advective and divergent heat, moisture and momentum tendencies for the single column model (SCM) atmosphere at 16 levels. The data were analyzed in 4-D VAR and made available at 3h intervals. We used the data to perform a 30 ensemble Control and 5 sets of ensembles of thirty cases each to examine the influence of soil moisture anomalies as described in section 3. The thirty soil moisture initializations were based on a 6-month simulation produced with ISLSCP Initiative I data for 1987 (a wet year that fits well with the wet summer of 1995) for each of the five soil types and six vegetation covers. Since the idea is to produce somewhat realistic soil moisture at the initial time, such a method is satisfactory for addressing the problem at hand. This is a compromise because the forcing data for the prior six months of 1995 was unavailable. We then performed the time series analysis and intercompare the simulations for each soil type and vegetation cover. The five sets of 30 runs each were produced in which the initial soil moisture profile varied by soil type only regardless of the vegetation fraction. The soil-moisture values were chosen to be the one for 60% vegetation cover (Fig.6) for the first set. The soil moisture deficit (saturation value (=1.0) minus the initial soil moisture at each of the 100-soil layers) was increased in steps of 25% for each of the subsequent four sets making it 100% more for the last set. This generated a total of 150 simulations. They were used to address more fully the influence of initial soil moisture on evapotranspiration and its influence on precipitation.

4.1 The Control Simulation

Figures 7a-c show the temperature, relative humidity, and precipitation errors (simulated minus

observed) at 3h intervals for soil type 3 and 60% vegetation cover -- a combination is nearest to the observed land-surface conditions. All other diagnostics akin to those discussed in Sud and Walker (1999) were produced and seemed realistic, but only three of those that could be verified against observations are shown. A fully interactive simulation with the same SCM, but with surface fluxes prescribed from observations without any other relaxation, were noted to be reasonably realistic (Ghan et al. 2000). The current simulation is fully interactive and has SSiB coupled to a 100-layer subsoil hydrology model (Koster et al., 2000). Naturally, it generates its own surface fluxes. However, the atmospheric simulation contains an additional adjustment for model errors as well as vegetation anomalies as discussed in Section 2. With these adjustments, it yields even more realistic time-mean atmospheric soundings, i.e., time series of the vertical profiles of temperature, Fig. 7a, and humidity, Fig. 7b. In the 3-week averages, (shown on the far right), the simulated time mean biases are at an acceptable level, while the instantaneous biases keep fluctuation about the mean. We note that there are two episodes of about 4^0C cooling with a preponderance of 1-2^0C warm (cool) patches at around 100 (400) hPa level, respectively. In the moisture field as well, there were no systematic biases. However, one could infer that near the surface the model atmosphere is a little too warm, which compensates for the cooler environments atop. However, recognizing that there is virtually no systematically growth in temperature error, we contend that the simulation is quite reasonable. Since the simulated precipitation is less than the observed (Fig. 7c), it implies either the simulated evaporation is too low or the horizontal moisture flux divergence is too high. As we will show, the evapotranspiration is quite realistic for the 60% vegetation cover, therefore the prescribed horizontal moisture convergence may be the culprit, and this could be caused by a model bias and/or the input data. Because these errors do not relate to any systematic errors in the accompanying fields, it seems to indicate that the model is performing well within the limits of observational errors.

The evapotranspiration and sensible heat flux time-series, shown in Fig. 8a & b, contain observations (black) and three vegetation cover cases with 1%, 60% and 99% vegetation (dashed

lines) for soil type 3. Some differences between the observed and simulated surface fluxes can not be explained by vegetation variations, but recognizing that the SCM has its own clouds, water vapor, long and short wave radiation parameterizations, the simulated fluxes can be considered realistic particularly because they depict good diurnal amplitudes and phases. The only purpose of showing them here is to convey to the reader that the SCM has the ability to simulate realistic surface fluxes and respond to rainfall episodes that suppress surface fluxes by cloud shielding of solar radiation. During the continued dry period: July 26, 1995 through July 30, 1995, the simulated sensible flux (evapotranspiration) is less (more) than the observed. This suggests that the parameterized vegetation had access to more soil moisture even though the simulated rainfall is lower. This is of some concern because it points to deficiency of the land model or biases in initial soil moisture profile (initialized with 1987 data), but the overall temporal structure of evapotranspiration is quite reasonable for addressing the current problem. Even though our model continues to produce reasonable precipitation time series for both cases (Fig. 8c) the current results show that the model can be considered satisfactory despite the 3-week mean precipitation being slightly less than the observed.

4.2 The Anomaly Simulation

As mentioned earlier, we used the SCM with above attributes to run 30 cases consisting of all possible combinations of 5 soil types (Fig 3b) and six discrete vegetation covers: 1, 20 40, 60, 80, 99%, respectively. The initial soil moisture profiles were determined from a 6-month soil moisture initialization run using 1987 ISLSCP Initiative I data. This compromise allows each soil-type and vegetation-cover combination to use an initial soil moisture profile appropriate for it, allowing us to address the problem of the influence of soil type and vegetation cover on precipitation using relatively more realistic initial soil moisture profile. A total of 150 simulations were subsequently used to establish the robustness of our findings to the initial soil moisture using arbitrary soil moisture anomalies as discussed above.

a) Evapotranspiration:

Figure 9a shows that the simulated evapotranspiration is a strong function of vegetation cover and soil type for the 3-week period. It is highest for soil type 5 and lowest for soil type 1. The relative patterns are robust regardless of the initial soil moisture-whether they are taken from 6-month initialization for each vegetation cover or from initial soil moisture for 60% vegetation cover case. The hydrologic characteristics of different soil types are distinguished mainly by soil water suction potential, ψ, and hydraulic conductivity, κ, as a functional of soil moisture fraction through:

$$\psi = \psi_s f_w^{-B}, \tag{8a}$$

and

$$\kappa = \kappa_s f_w^{2B+3}, \tag{8b}$$

where ψ_s and κ_s are the corresponding saturated soil values; f_w is the soil moisture fraction and B is Clapp and Hornberger (1978) parameter. An increase in evapotranspiration for a larger vegetation cover would be expected naturally, but its dependence on soil type is determined by ψ_s and B functions. The only major exception is soil type 5 for which it reduces for 80% and 100% vegetation covers. This can be the result of non-linear stomatal control of vegetation to soil moisture, ambient temperature and the PAR (Photosynthetically Active Radiation). Such a combined non-linear behavior is not so easy to discern in simple theoretical arguments and is beyond the purview of the current focus. The accompanying sensible fluxes (not shown) were consistent with the surface energy balance and do not have large variations. We naturally expect sensible fluxes to decrease with increasing vegetation cover, but this is intertwined into solar energy absorption at the surface through the surface albedo, α_{surf} given by:

$$\alpha_{surf} = V_f \alpha_{forest} + (1 - V_f)\alpha_{desert}, \tag{9}$$

while its transpiration characteristics are modulated by the limiting influence of wilting for

low levels of root zone soil moistures. The interactions lead to a slight increase in sensible fluxes with increased vegetation, particularly for soil type 3. It is quite possible that lack of the dependence of surface albedo of the soil on the top layer soil moisture is responsible for this behavior.

b) Precipitation:

The dependence of precipitation on evapotranspiration due to changes in vegetation cover and soil type very much affirm the qualitative inferences of Sud et al. (1993 & 1995) and Schickedanz and Ackermann (1977). It is shown in the corresponding panels on the right hand side of Figure 9a. The simulated precipitation increases with increased vegetation cover as well as evapotranspiration. One case of soil type 5 in which the evapotranspiration decrease for 80% vegetation cover shows a corresponding decrease in precipitation. The spread among the different soil types becomes less as vegetation cover increases. As expected, for high vegetation cover, e.g., 99%, both the evaporation and precipitation for all soil types tend to be significantly closer. These results suggest that the influence of the soil type on evapotranspiration get suppressed as vegetation controls influence evaporation. We match of evapotranspiration with observations but the simulated precipitation continues to be less than the observed. The error does not seem to be related to moisture storage in the atmosphere because the model was shown to simulate realistic temperatures and specific humidity profiles (see Section 4.1). Hence, the discrepancy must emanate from the prescribed (ARM-CART data) or model bias correcting for the horizontal advection (Eq.5, section 2) of moisture. It implicates input data and/or the adjustment process itself correcting for SCM biases. Nevertheless, for a given vegetation cover, the soils that produce more evapotranspiration also produce more precipitation is abundantly evident in these simulations.

c) Vegetation-Evaporation-Precipitation Relationships

Here we expand on the main theme of the evapotranspiration-precipitation relationship as a

function of change in vegetation cover and initial soil moisture as well as $\Delta P/\Delta E$. First, we took the original ensemble of 30 control runs. We plotted the increases in E and P relative to 1% vegetation cover for soil type-3 alone as well as the means for all 5-soil types (Figure 9b). The corresponding $\Delta P/\Delta E$ is also shown in the Figure. The relationships between evaporation and rainfall increases as a function of vegetation cover are not so straight forward to interpret; nevertheless, $\Delta P/\Delta E$ values remain between 40-60% range, a result that is more clearly borne out in the next set of soil moisture controlled simulations. Subsequently, we produced the same analysis for 150 simulations in which the initial soil moisture was based on the 60% vegetation cover soil moisture initializing runs. The 5-ensembles corresponding to five soil moisture initial conditions (described before) were again used to produce ΔP and ΔE and $\Delta P/\Delta E$ for each of the five ensembles and averaged for all the soil types. These provided a very coherent and robust picture (Figure 9c). Since the input data, including moisture divergences, are prescribed from the ARM-CART data and is identical for each of the 150 simulations, the simulations remain heavily constrained by the prescribed large-scale flow. Nevertheless, it is modulated by evapotranspiration anomalies due to vegetation cover through equations (4a & b) and soil moisture effects. One clearly sees how vegetation cover affects the evapotranspiration, precipitation, and the ratio $\Delta P/\Delta E$. Vegetation helps to access the deep soil moisture, but with stomatal controls the influence of initial soil moisture on the increase in evapotranspiration are highly non-linear. Nevertheless, the relationship of precipitation change in response to evapotranspiration change is quite robust. It shows as a positive feedback with about 40-60% recovery of evapotranspiration increase through precipitation income. The results are quite similar for each soil type (not shown) and even for different initial soil moisture values.

d) Evaporation-Precipitation Relationship

Figure 10a shows the 3-week averaged evaporation-precipitation plot for all 180 simulations. It shows that atmosphere responds to evaporation change in a robust fashion regardless of the complexity of the biospheric processes and land-hydrology. This response is delightfully simple and linear. It helps us infer that for the Great Plains region, roughly 50% of the evapotranspiration is returned back in the form of increased precipitation. Indeed regression analysis gave a slope of 0.499, which as a rule of thumb can be round off to 50%. We attempted to verify the intercept of 5.06 mm d^{-1} precipitation dry soil case by running one simulation with zero initial soil moisture. However, the simulation produced an evaporation of 0.47 mm d^{-1} through evaporation of rainfall interception and soil surface wetting. The corresponding simulated precipitation was 5.26 mm d^{-1} (plotted as black dot in Figure 10a). This case too affirms the simple straight line relationship.

e) Moisture distribution in the Vertical

(i) Vegetation Dependence

The vertical structure of moisture divergence has some interesting features, Fig. 10b. In response to increased vegetation cover, the moisture divergence becomes smaller near the surface, i.e., between 960 (surface pressure) and 850 hPa. However, it increases for the middle atmosphere, i.e., between 500 and 850 hPa. In other words despite higher evapotranspiration with increased vegetation cover, the horizontal moisture divergence reduces. The difference is due to enhanced upward transport of moisture by physical processes and/or removal by low-level condensation (truly small). An increase in moisture divergence in the middle atmosphere represents the influence of moist convection and dry turbulent exchanges. These results are naturally complicated by surface albedo decreases for higher vegetation cover. Indeed, higher surface energy fluxes would amount to larger moist static energy and invigorated moist convection. However, in view of 30 different spin ups of initial soil moisture, the land with lower vegetation cover naturally builds up

higher soil moisture and tries to mitigate evapotranspiration reduction produced by lesser vegetation cover. Since, a layer moistened with increased evaporation is expected to produce higher moisture divergence, the simulated reduction in moisture divergence suggests the dominant role of upward moisture transport by physical processes. In fact not only the moist convection would transport the moist air up, but it also brings dry air into the near surface layers through convective scale downdrafts. To the extent that the moisture loss of lower layer is reflected as moisture gain in the middle layer or even top layer (which is miniscule), it is the outcome of the vertical transport. The difference between these represents the increase in moisture divergence. Indeed, when we increased the depth of the lower layer to 700mb, most of the moisture divergence changes were reflected in the lowest layer (not shown). In this way, we note that surface fluxes can affect the vertical transport of the moisture through the boundary layer and moist convective processes and reveal that despite the evaporation increase, the layer can dry.

(ii) Evapotranspiration Dependence

The simulation can be examined also by looking at the dependence of near surface moisture divergence on evapotranspiration. Such a result is much easier to interpret. The scatter plot in Fig. 11 shows a discernible scatter because the surface energy absorption is a function of vegetation cover and that also influences the surface evaporation. As expected, the moisture divergence reduces as evapotranspiration increases. This is obviously different from its relationship with vegetation cover where it reduced with vegetation cover that is responsible for evaporation increase. The upper level moisture divergences, i.e., 850-200 hPa (not shown), have compensating (opposite sign) effects on the moisture divergence simulated in the near surface layers (shown in Fig. 11). The sum of the entire column moisture divergences yields a smooth graph showing a linear relationship between moisture divergence and evapotranspiration. This is also consistent with a linear relationship between simulated precipitation and evapotranspiration shown in Fig 10a.

5. Discussion and Conclusion.

The aim of the current investigation is to broadly understand the evaporation-rainfall relationship together with the role of soil types, vegetation cover and initial soil moisture. If the precipitation were weakly affected by evapotranspiration, the rainfall in the region would be largely independent of evapotranspiration. One can intuitively infer that Sahara Desert and/or coastal regions with orographic lifting and inland large-scale flow would be such regions. But how does the relationship vary in different regions; and how are regions with strong evaporation-precipitation feedback distributed around the world and where would one have the ability to influence the precipitation by clever management of the biosphere remains a puzzle to be addressed and understood.

All the current single column model simulations for the ARM-CART data confirm a positive feedback between evapotranspiration and precipitation. However, there were no cases in which precipitation increase exceeded the evapotranspiration increase. Such an occurrence would generate a runaway wet environment and evidently early summer season of the mid-western United States is not a candidate for such an outcome. We simulate larger evapotranspiration in the growing season in response to higher initial vegetation cover. The extra water needed for increasing the evapotranspiration would have to be supplied through irrigation that draws from external water sources or ground water storage. However, because of the evapotranspiration-rainfall relationship and efficient retention of rainfall water by the vegetation in the biosphere, the external water supply needs to be roughly half of that needed for supplementing evapotranspiration. Obviously, these results can not be generalized to other regions. Even for the mid-west July, the new results warrant some caution. First we need to establish the robustness of these results with more cases. Second, we prescribed the large-scale flow to the SCM. This assumes that the regional hydroclimatological changes are not so large as to affect the large-scale. This might not hold good on all scales. Nevertheless, we have made an appropriate adjustment

for the large-scale forcing of the SCM by introducing a methodology for the grid-scale columnar temperature and humidity changes to affect their advective tendencies in the horizontal as well as the vertical directions. Consequently, we contend that our study addresses a realistic case study in which scale-separation between the large and meso-scales has been assumed.

Indeed, the moisture advected out of the SCM will not a total loss for the United States because it has a long way to travel before it leaves the continent. It naturally augments the specific humidity of the air mass flowing out of the region and is likely to increase the precipitation in the nearby regions (Schickedanz, and Ackermann, 1977). For this reason even if the irrigation relies on water that is available a few hundred kilometers around the region, the excess rainfall outside the region is likely to recover some of the water usage.

A natural question is: would the increase in sub-grid scale sensible flux and moist processes anomalies due to changes in vegetation cover and evapotranspiration not affect the local meso-scale circulation? The answer is: indeed, it would (Pielke and Avissar, 1990), but the goal of a good parameterization is to handle such effects realistically, particularly in the domain-averaged sense. Whether our SCM invoking GEOS II physics and McRAS has good enough parameterizations to address such influences remains unanswered, but the fact that the SCM responds realistically to several ARM-CART and other evaluations provides some credibility to these studies (Sud and Walker, 1999, and Ghan et al., 2000). Besides, SSiB and its evapotranspiration sub-model have been evaluated thoroughly with several field observations while the new 100-layer land hydrology model in invoked to improve the hydrologic accuracy of soil-water conduction. Therefore, we are convinced that our evapotranspiration and soil hydrology model is as good as any modern state-of-the art SCM can provide. We believe, studies such as this help to alleviate some of the confusion created by a variety of answers given by GCMs to a typical deforestation such as summarized in Hahmann and Dickinson (1997) and other studies of climatic effects of vegetation and/or soil-moisture anomaly scenario.

In addition to the above limitations of the evaluation procedure and modeling assumptions, several inherent parameterization problems continue to hinder an accurate simulation of a land-atmosphere interaction. Among the unsolved problems are the influences of subgrid-scale effects that include small-scale variability of soil type, soil moisture, as well as the natural and agricultural biodiversity, orography and related natural drainage characteristics, and surface runoff pathways with its associated effects on the water table and soil moisture availability. A highly non-linear response of surface fluxes to such variations makes the problem of parameterizing land processes truly hard-to-address. In addition the intrinsic variability of biospheric processes, particularly on climatic time-scales, diminishes the positive influences of these advances on the improved climate simulation even though interactive biosphere climate simulations have begun to show promise (Zeng et al., 1999). Under the circumstances, controlled evaluations such as ours may provide a useful answer. We plan to continue to test our new results with additional datasets and regional model exercises for the mid-west and other important regions of the world.

Acknowledgments: The funding support of our research by Dr. Kenneth Bergman of NASA headquarters is immensely appreciated. Participation of two co-authors, D. M. Mocko and G. K. Walker was supported by these funds. Dr. W. K.-M. Lau, Head Climate and Radiation Branch of the Laboratory for Atmospheres encourages this research.

REFERENCES

Anthes, R. A., 1984: Enhancement of convective precipitation by mesoscale variations in vegetative covering in semi-arid regions. *J. Clim. and Appl. Meteor.* **23**, 4, 541-554.

Arakawa, A. and W. H. Schubert, 1974: Interaction of a cumulus ensemble with the large-scale environment, Part I. *J. Atmos. Sci.*, **31**, 674-701.

Avissar, R., 1992: Conceptual aspects of a statistical-dynamic approach to represent landscape subgrid-scale heterogeneities in atmospheric models . J. Geophys. Res., **97,** D3: p. 2729-2742.

Clapp, R. B. and G. M. Hornberger, 1978: Ensemble equations for some soil hydraulic properties. Water Resources Res., **14**, 4, 601-604.

Cheng, M.-D., 1989: Effects of downdrafts and mesoscale convective organization on the heat and moisture budgets of tropical cloud clusters. Part I: A diagnostic cumulus ensemble model. *J. Atmos. Sci.*, **46**, 1517-1538.

Dickinson, R. E., 1980: Effect of tropical deforestation on climate. Blowing in the wind: deforestation and long range implication, studies in the third world societies, Pub. No. **14**, *Dept. Anthropology, College of William and Mary*, 411-441.

Dickinson, R. E., and A. Henderson-Sellers, 1988: Modeling Tropical Deforestation: A study of GCM land surface parameterizations. *Quart. Jour. Roy. Meteor. Soc.*, Vol. **114**, 439-462.

Dirmeyer, P. A., and J. Shukla, 1994: The effect on climate of doubling deserts. Center for Ocean-Land-Atmosphere Studies, 4041 Powder Mill Road, Suite 302, Calverton, MD 20705-3106. Report No. **3**. 32pp.

Dirmeyer, P. A., A. J. Dolman, and N. Sato, 1999: The pilot phase of the global soil wetness project. *Bull. Amer. Meteor. Soc.*, **80**, 5, 851-878..

Eltahir, E. A. B., and R. L. Bras, 1993: On the response of tropical atmosphere to large-scale deforestation. Quart. J. Roy. Meteor. Soc., 119, pp. 779-793.

Ghan S. J, Randall D, Xu K, Cederwall R, Cripe D, Hack J, Iacobellis S, Klein S, Krueger S, Lohmann U, Pedretti J, Robock A, Rotstayn L, Somerville R, Stenchikov G, Sud Y, Walker G, Xie S, Yio J and

Zhang M, 2000: A Comparison of Single Column Model Simulations of Summertime Midlatitude Continental Convection". J. Geophys. Res.. D. **105** (D2), 2091-2124.

Hahmann, A. N., and R. E. Dickinson, 1997: RCCM2-BATS model over tropical South America: Application to tropical deforestation. J. Cimate, **10**, 8, 1944-1964.

Henderson-Sellers, A., R. E. Dickinson, T. B. Durbidge, P. J. Kennedy, K. McGuffie and A. J. Pitman, 1993: Tropical deforestation – Modeling local-scale to regional-scale climate change. *J. Geophys. Res.*, **98**, D4, 7289-7315.

Hoffert, M. I., and Y. C. Sud, 1976: Similarity theory of the buoyantly interactive planetary boundary layer with entrainment, Jour. Amos. Sci., **33**, 11, 2136-2151.

Koster, D. K., and P. S. Eagleson, 1990: A one dimensional interactive soil-atmosphere model for testing formulations of surface hydrology. *Jour. Clim.*, **3**, 6, 593-606.

Koster, D. K., and M. J. Suarez, 1999: A simple framework for examining the interannual variability of land surface moisture fluxes. *Jour. Clim.*, **12**, 7, 1911-1917.

Koster, R. D., M. J. Suarez, A. Ducharne, M. Stieglitz, and P. Kumar, 2000: A catchment-based approach to modeling land surface processes in a GCM, Part 1, Model Structure, J. Geophys. Res. (Submitted).

Mocko, D. M., and Y. C. Sud, 1998: Comparison of land surface model (SSiB) to three parameterizations of evapotranspiration-a study based on the ISLSCP Initiative I data. Earth Interactions, **2**, 40pp.

Moorthi, S. and M. J. Suarez, 1992: Relaxed Arakawa-Schubert: A parameterization of moist convection for general circulation models. Mon. Wea. Rev. **120**, 978-1002.

Nicholson, S. E., 1985: Sub-Saharan rainfall 1981-1984. J. Clim. Appl. Meteorol., **24**, 1388-1391.

Otterman, J., A. Manes, S. Rubin, P. Alpert, D. O'C. Starr, 1990: An increase of early rains in southern Israel following land-use change. Bound- Layer Meteor., **53**: 331-351.

Pielke, R. A. R. Avissar, 1990: Influence of landscape structure on local and regional climate. Landscape Ecology, **4:** 133-155.

Randall, D. A., K.-M. Xu, R. J. C. Somerville, and S. Iacobellis, 1996: Single column models and cloud ensemble models as links between observations and climate models, J. Climate, **9**, 8, 1683-11697.

Randall, D. A., and D. G. Cripe, 1999: Alternative methods for specification of observed forcing in single-column models and cloud system models. J. Geophys. Res, **104**, 24527-24545.

Schickedanz, P. T., and W. C. Ackermann, 1977: Influence of irrigation on semi-arid climates, Based on the International Symposium, 16-21 February 19765, Alexandria, Egypt. Pergamon Press, p 185-196.

Skole, D., and C. Tucker, 1993: Tropical deforestation and Habitat fragmentation in the Amazon: Satellite data from 1978 to 1988. *Science*, **260**, 1905-1910.

Sud, Y. C. and M. J. Fennessy, 1982: A study of the Influence of Surface-albedo on July circulation in semi-arid regions using the GLAS GCM, Jour. Climatology, **2**, 105-125.

_____, and Fennessy, M. J., 1984: A numerical study of the influence of evaporation in semi-Arid regions on the July circulation. J. Climatol., 4, 383-98.

_____, and W. E. Smith, 1985: Influence of land-surface processes in the Indian Monsoon-a numerical study. J. Clim. Appl. Meteor., **24**, 10, 1015-1036.

_____, and A. Molod, 1988: A GCM simulation study of the influence of Saharan Evapotranspiration and Surface-Albedo anomalies on July circulation and rainfall. Mon. Wea. Rev.,**116**: 2388-2400.

_____, W. C. Chao, and G. K. Walker, 1993: Dependence of Rainfall on vegetation: theoretical considerations, simulation experiments, observations, and inferences from simulated atmospheric soundings. Jour. Arid-Environ., **25**, 5-18.

_____, and G. K. Walker, 1993: A rain-evaporation and downdraft parameterization to complement a cumulus updraft scheme and its evaluation using GATE data. Mon. Wea. Rev. **121**, 11, 3019-3039.

_____, K.-M. Lau, G. K. Walker, and J. H. Kim, 1995: Understanding biosphere-precipitation relationship: Theory, model simulations and logical inferences, Mausam, 1-14.

_____, and G. K. Walker, 1999: Microphysics of Clouds with the relaxed Arakawa-Schubert Scheme (McRAS). Part I Design and Evaluation with GATE Phase III data. J. Atmos. Sci., **56**, 18, 3196-3220.

Sundqvist, H., 1988: Parameterization of condensation and associated clouds in models for weather prediction and general circulation simulation. In: *Physically based modelling and simulation of climate and climatic change*, (ed. M. E. Schlesinger), Riedel, Dordrecht, Part 1, 433-461.

Sundqvist, H., E. Berge, and J. E. Kristjansson, 1989: Condensation and cloud parameterization studies with a

mesoscale numerical weather prediction model. *Mon. Wea. Rev.*, **117**, 1641-1657.

Sundqvist, H. E., 1993: Inclusion of ice-phase of hydrometeors in cloud parameterization of large-scale and meso-scale models. *Contr. Atmos. Phys.*, **66**, 137-147.

Walker, G. K., Y. C. Sud, and R. Atlas, 1995: Impact of the ongoing Amazonian deforestation on local precipitation: a GCM simulation study, Bull Amer. Meto. Soc., 76, 346-361.

Xue, Y. K., P. J. Sellers, J. L. Kinter III, and J. Shukla, 1991: A simplified Biosphere model for global climate studies, J. Climate, **4**: 345-364.

Zeng, N., J. D. Neelin, K.-M. Lau, and C. J. Tucker, 1999: Enhancement of interdecadal climate variability in the Sahel by vegetation interaction. Science, 286: (5444) 1537-1540.

Figure Legends

Figure 1. Schematic representation of convective, stratiform and boundary layer clouds in McRAS ***(Adapted from Sud and Walker, 1999).***

Figure 2. SCM testing of McRAS with ARM-CART datasets for Case 1 and Case 3. Figure 2a through 2c show simulation errors for the temperature, specific humidity, and precipitation fo the SCM-region.

Figure 3a. Coupling of a100-layer soil hydrology and SSiB with schematic fluxes.

Figure 3b. Soil types in ISLSCP Initiative one data depicted in the three-component mixture viewed as soil triangle. Typical mixing ratios of the soils are located in the triangle.

Figure 4. Influence of vegetation cover on the hydrology and surface fluxes simulated for 1987 with the ISLSCP Initiative 1 data of the Oklahoma region (a surrogate for ARM-CART site). Fig 4a shows actual fields and Fig 4b shows vegetation anomaly minus Control differences.

Figure 5 Same as Fig.4 except for Sahel region.

Figure 6. Thirty Initial-time soil-moisture profiles for all case studies. These soil-moistures are produced by running each of the five soil types with each of the six vegetation covers for six months: January 1 through July 1, with ISLSCP Initiative I forcing data for 1987.

Figure 7. Simulated error time-series for the Control case: Soil Type 3 and vegetation cover of 60% with corrections for the model errors: (a) Temperature fields; (b) humidity fields; and (c) simulated vis a vis observed precipitation.

Figure 8. Soil Type 3 simulated vis a vis observed fluxes of (a) evapotranspiration and (b) sensible heat. The corresponding precipitation is in 8c. The three lines are for 1%, 60%, and 99% vegetation covers versus observations, which correspond to roughly 60% vegetation cover.

Figure 9a. Simulated evaporation and precipitation for the 3-week period for each of the six vegetation types using (top) different soil moisture spin up profiles, and (bottom) 60% vegetation cover Initial Soil Moisture Profile.

Figure 9b. Same as figure 9b except for a comparison of Soil Type 3 with that of the average of all soil types. In this figure the initial soil moisture profiles were the ones from Fig. 6.

Figure 9c. Evaporation and precipitation increases as a function of vegetation fraction with prescribed Initial soil moisture profiles. Averaged results for all five soil types are used to make the plots. $\Delta p/\Delta E$ is plotted on top and shows a very robust 40-60% recovery of increased evaporation through precipitation.

Figure 10a. Evaporation Precipitation Relationship for an ensemble of 5-sets in which each set has 5 soil types, six vegetation covers and an initial soil moisture profile from 60% vegetation-cover initialization produced with a 6-month spinup shown in Fig. 6. .

Figure 10b Averaged moisture divergence between (i) surface and 850 hPa, (ii)850 and 500 hPa, (iii) 500-200 hPa, and (iv) entire column values as a function of vegetation cover for simulation with initial soil moisture profiles of Fig.6.

Figures 11 Scatter plots of (i) surface-850 hPa level moisture divergence and (ii) total column moisture divergence as a function of surface evaporation regardless of the vegetation fraction or initial soil moisture.

Fig. 1

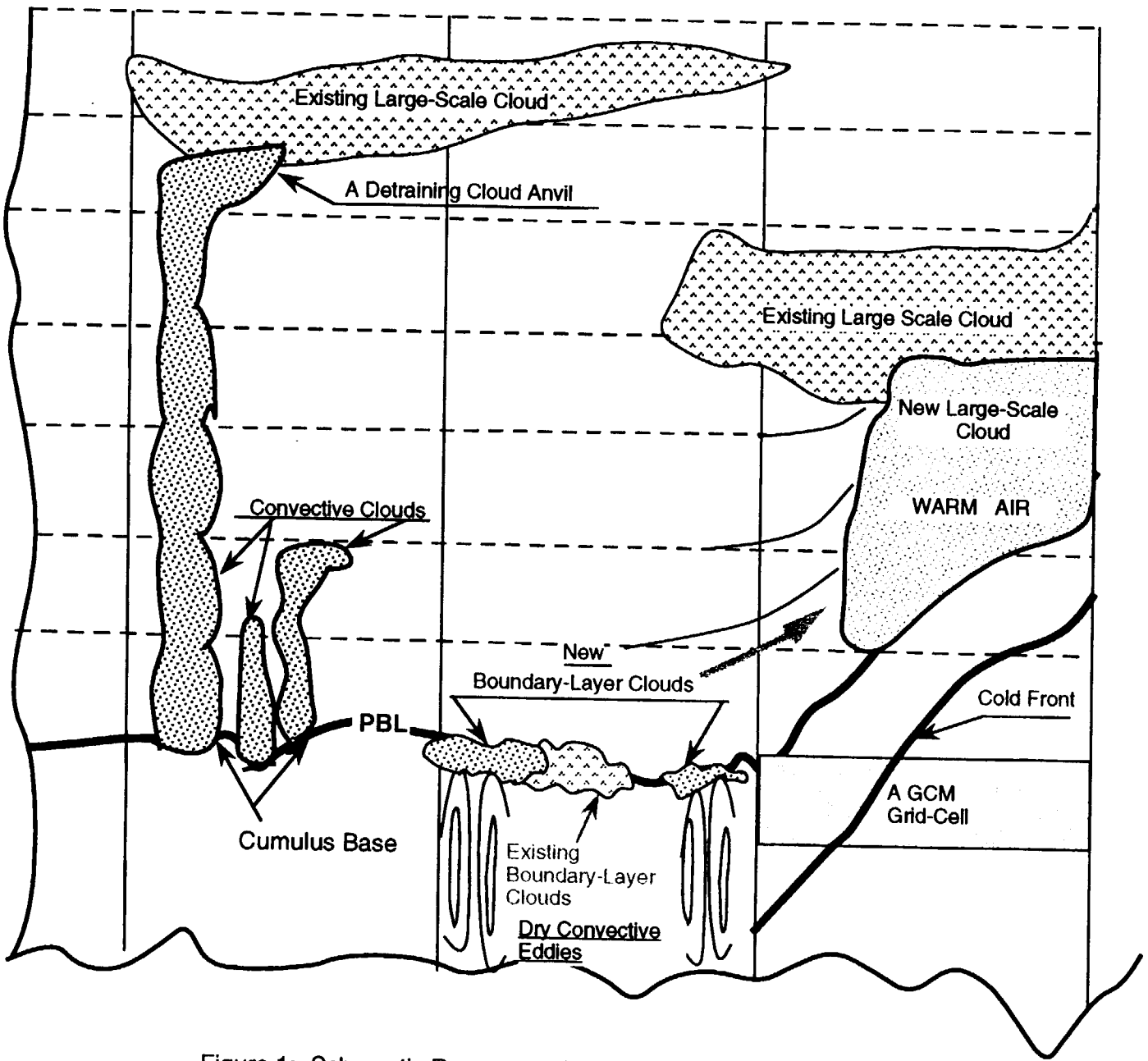

Figure 1: Schematic Representation of Different Clouds in the GCM

Fig 2a

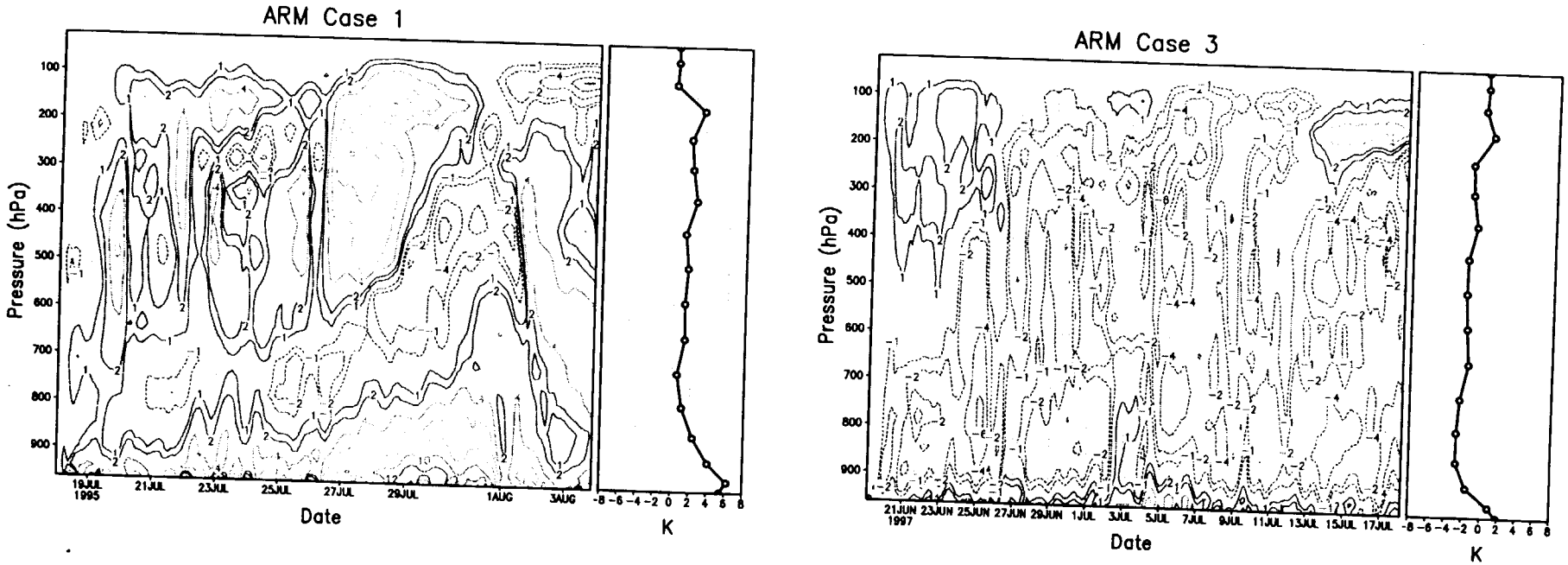

Figure 2a. SCM Simulated Temperature Errors for 2 case studies

Fig 2b

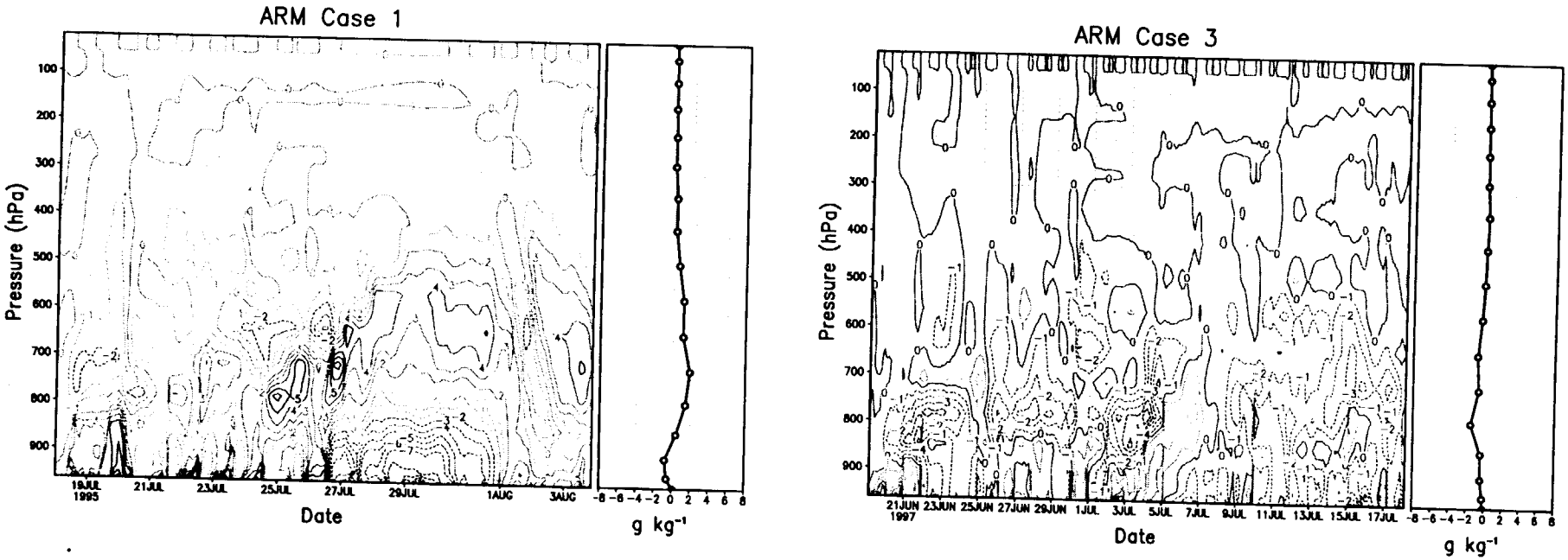

Figure 2b. SCM Simulated Specific Humidity Errors for 2 case studies

Fig 2c

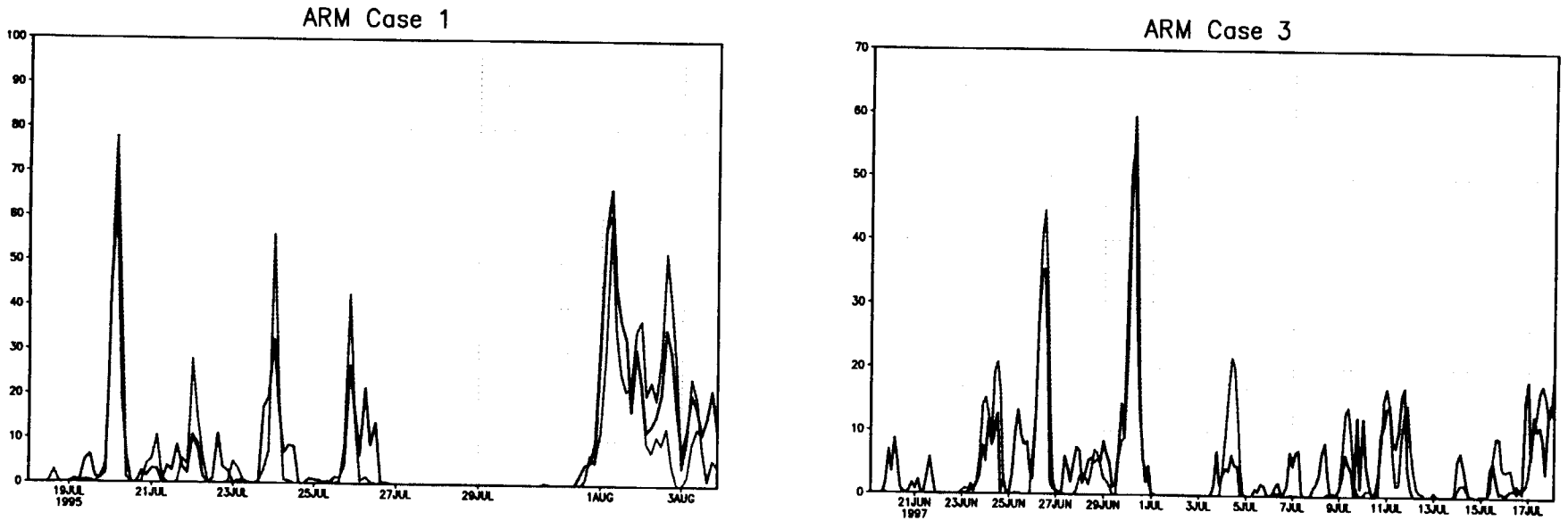

Figure 2c. SCM Simulated and Observed Precipitation (mm day^{-1}) for 2 case studies.

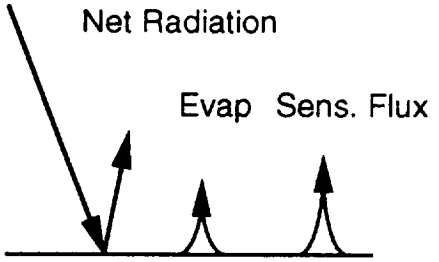

Soil-Layer of about 50 cm thickness

SINGLE LAYER SLAB

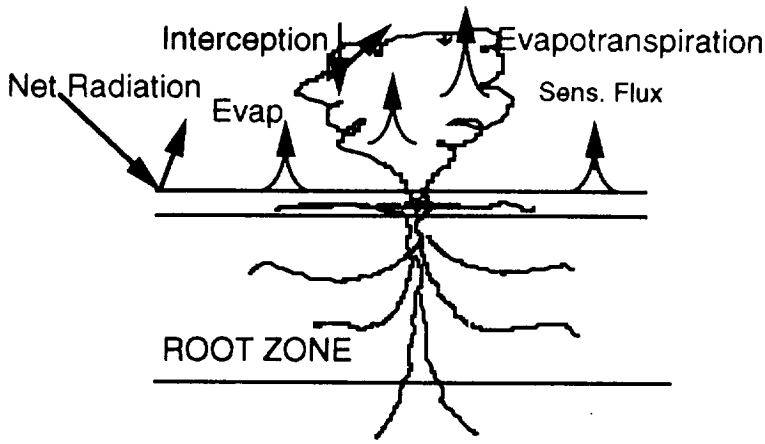

DEEP LAYER

3-LAYER SSiB MODEL

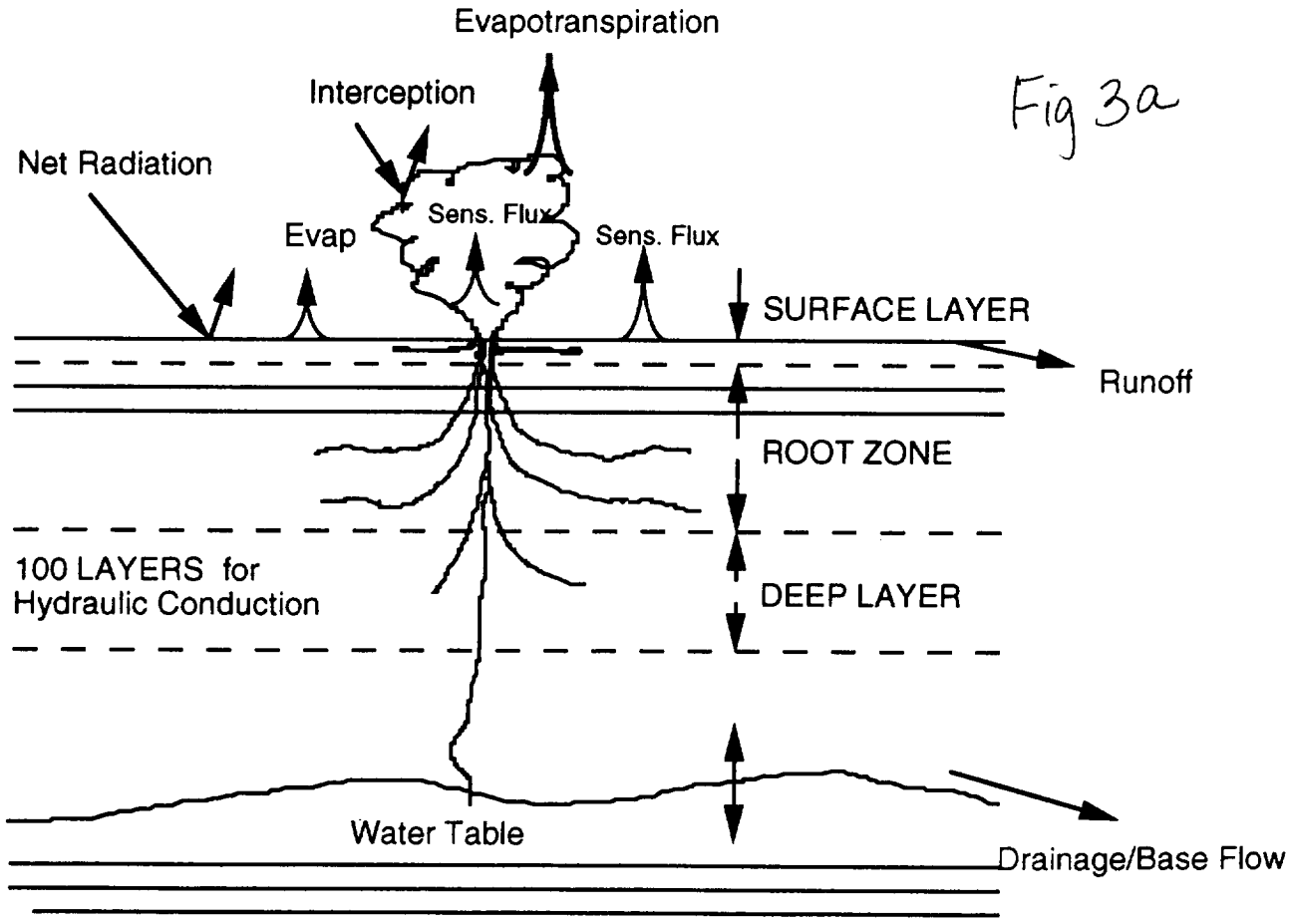

Fig 3a

SSiB WITH INTERACTIVE WATER TABLE(HY-SSiB)

Figure 3a

Soil types and parameters in ISLSCP Initiative I GEWEX GSWP dataset.

Soil Type	Index	Porosity	$\psi_s(m)$	$\kappa_s(m/s)$	B
Coarse - Loamy Sand	1	0.421	.0363	1.41E-5	4.26
Medium Coarse - Sandy Loam	2	0.434	.1413	5.23E-6	4.74
Medium - Loam	3	0.439	.3548	3.38E-6	5.25
Fine Medium - Sandy Clay Loam	4	0.404	.1349	4.45E-6	6.77
Fine - Clay Loam	5	0.465	.2630	2.45E-6	8.17

Table 1 + Fig 3b.

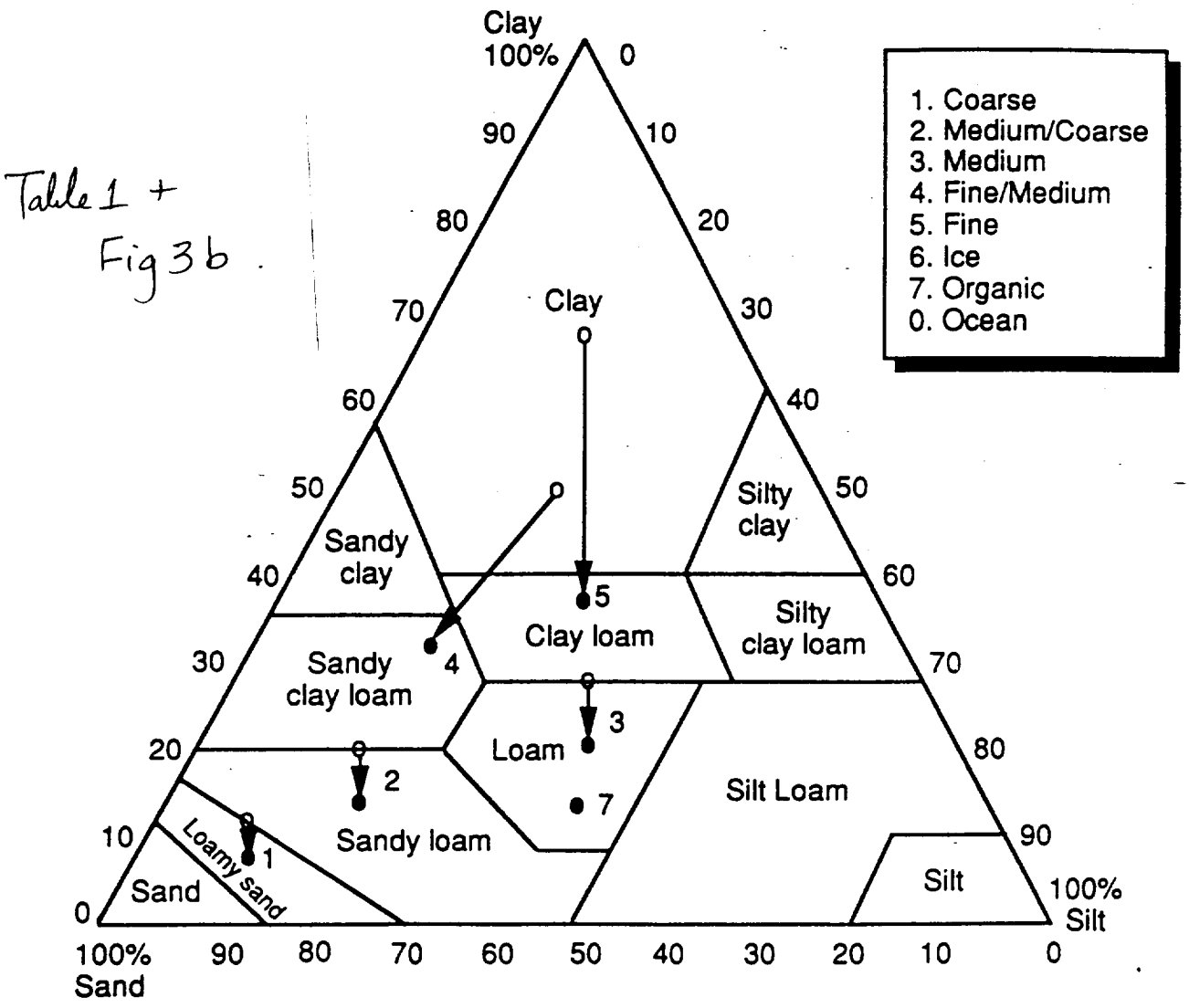

Fig 4a

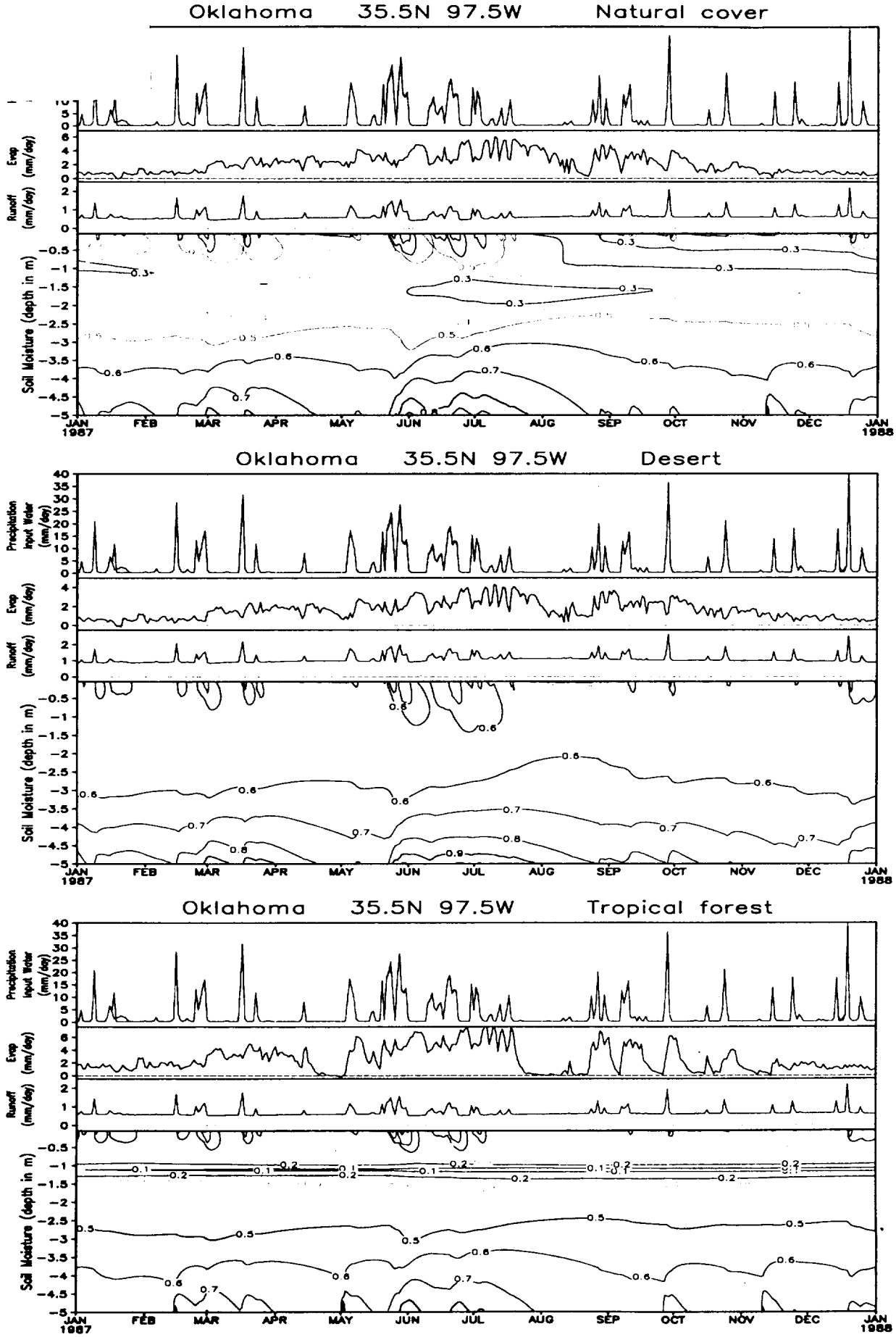
Oklahoma 35.5N 97.5W Natural cover
Evap (mm/day)
Runoff (mm/day)
Soil Moisture (depth in m)
JAN 1987
FEB
MAR
APR
MAY
JUN
JUL
AUG
SEP
OCT
NOV
DEC
JAN 1988
Oklahoma 35.5N 97.5W Desert
Precipitation Input Water (mm/day)
Evap (mm/day)
Runoff (mm/day)
Soil Moisture (depth in m)
Oklahoma 35.5N 97.5W Tropical forest
Precipitation Input Water (mm/day)
Evap (mm/day)
Runoff (mm/day)
Soil Moisture (depth in m)

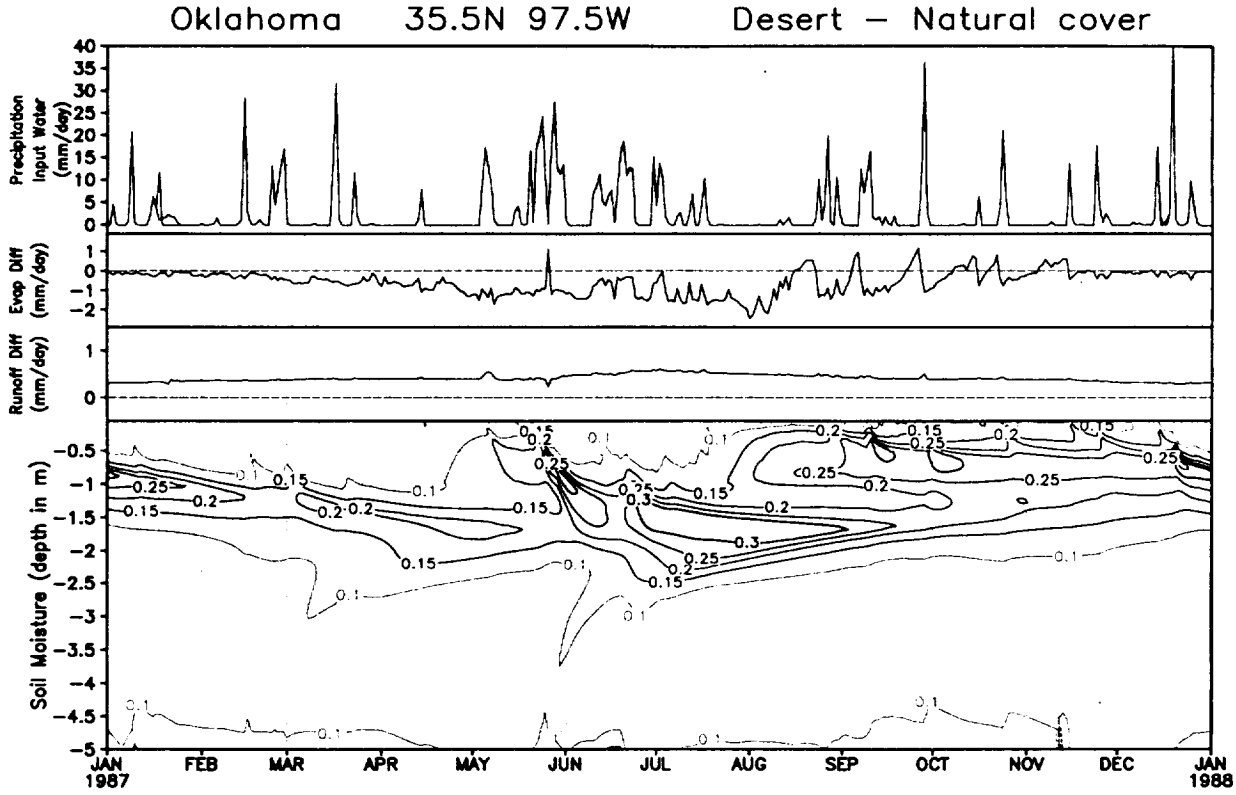
Oklahoma 35.5N 97.5W Desert – Natural cover
Precipitation Input Water (mm/day)
Evap Diff (mm/day)
Runoff Diff (mm/day)
Soil Moisture (depth in m)
JAN 1987
FEB
MAR
APR
MAY
JUN
JUL
AUG
SEP
OCT
NOV
DEC
JAN 1988

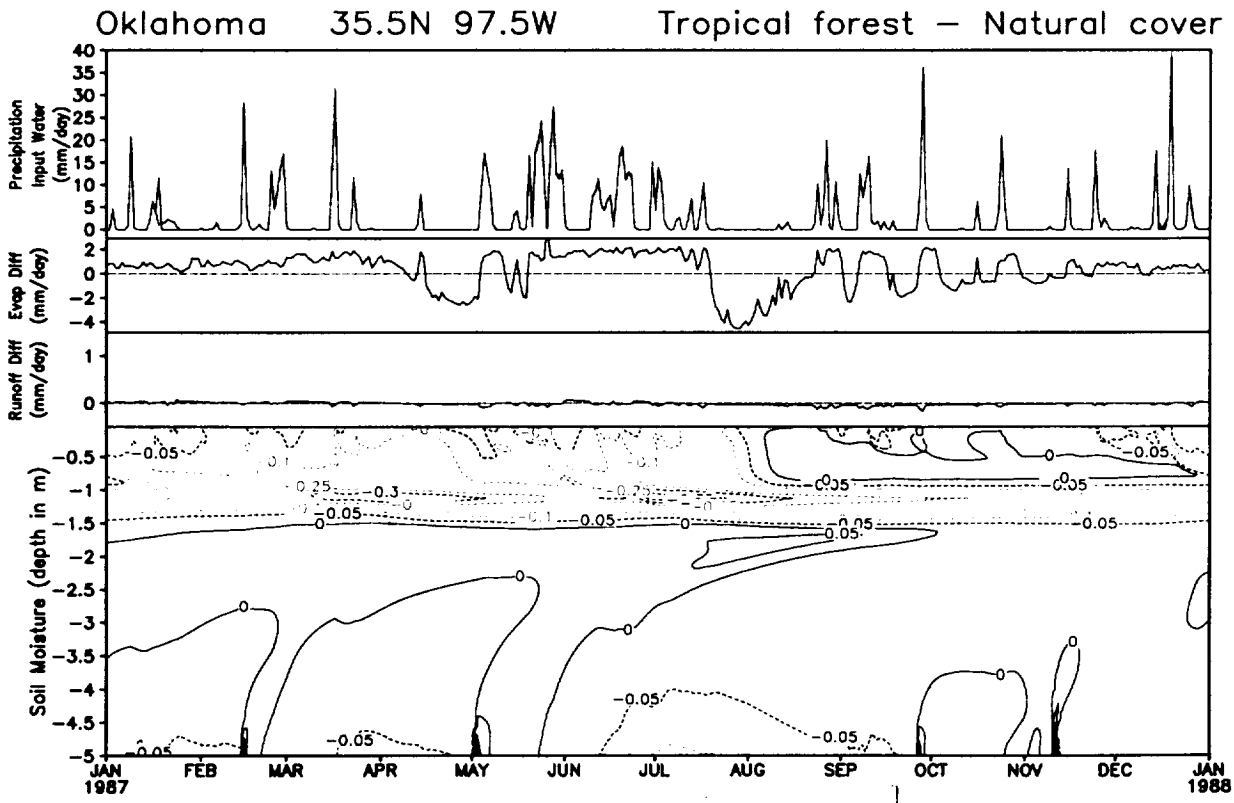
Oklahoma 35.5N 97.5W Tropical forest – Natural cover
Precipitation Input Water (mm/day)
Evap Diff (mm/day)
Runoff Diff (mm/day)
Soil Moisture (depth in m)
JAN 1987
FEB
MAR
APR
MAY
JUN
JUL
AUG
SEP
OCT
NOV
DEC
JAN 1988

Fig 4b

Fig 5a

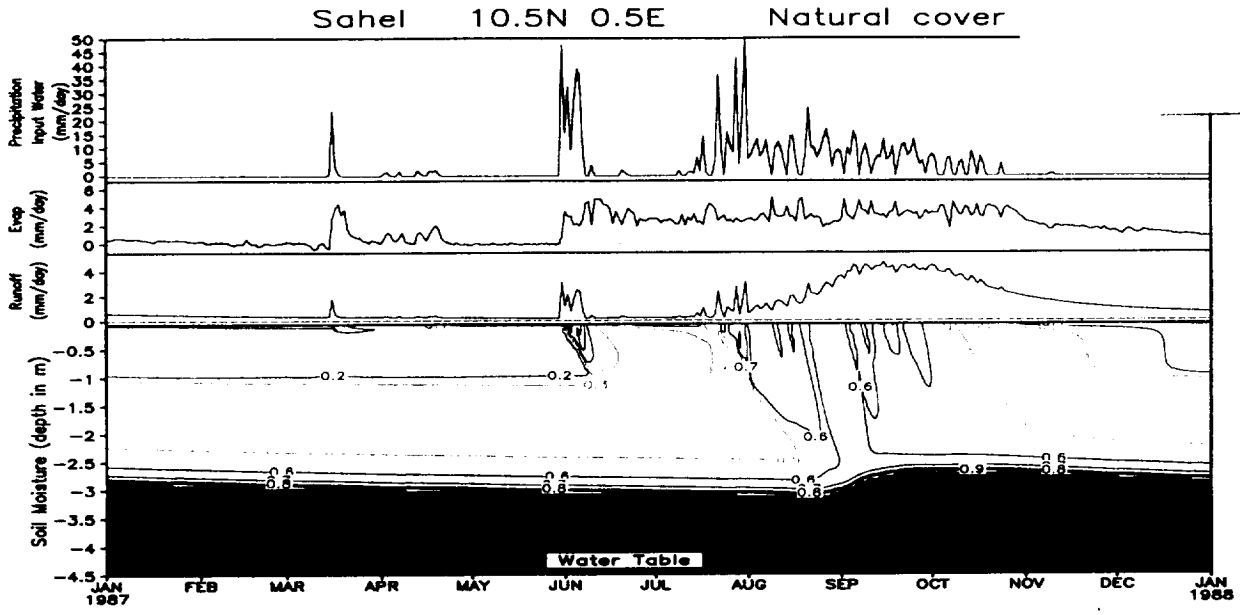
Sahel 10.5N 0.5E Natural cover
Precipitation Input Water (mm/day)
Evap (mm/day)
Runoff (mm/day)
Soil Moisture (depth in m)
Water Table
JAN 1987
FEB
MAR
APR
MAY
JUN
JUL
AUG
SEP
OCT
NOV
DEC
JAN 1988

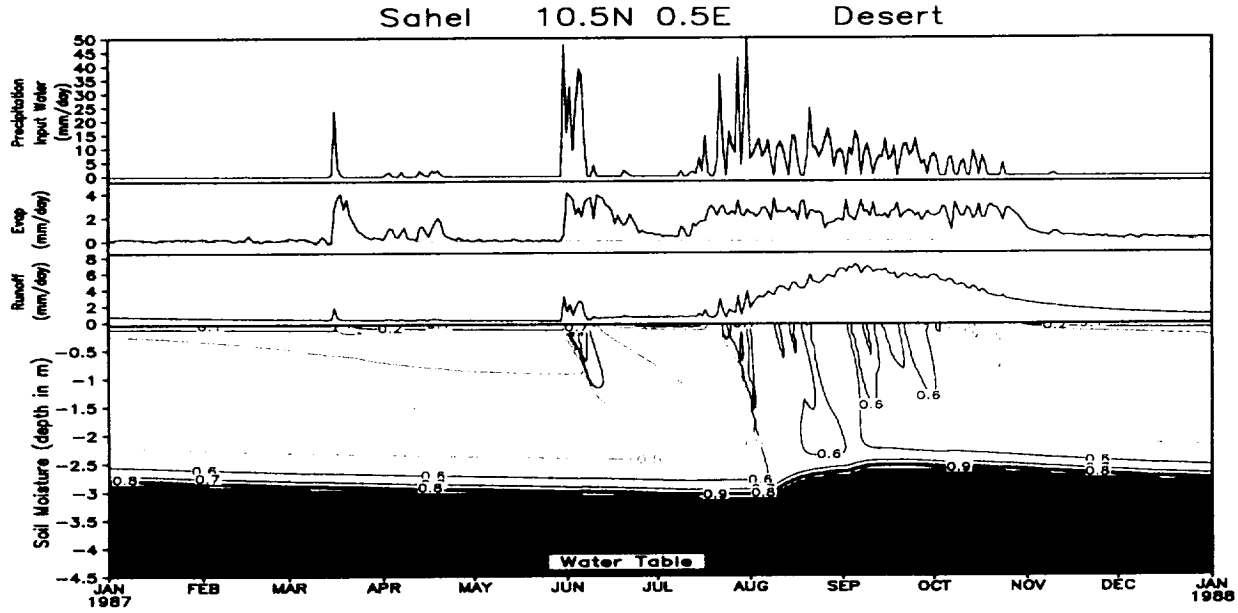
Sahel 10.5N 0.5E Desert
Precipitation Input Water (mm/day)
Evap (mm/day)
Runoff (mm/day)
Soil Moisture (depth in m)
Water Table
JAN 1987
FEB
MAR
APR
MAY
JUN
JUL
AUG
SEP
OCT
NOV
DEC
JAN 1988

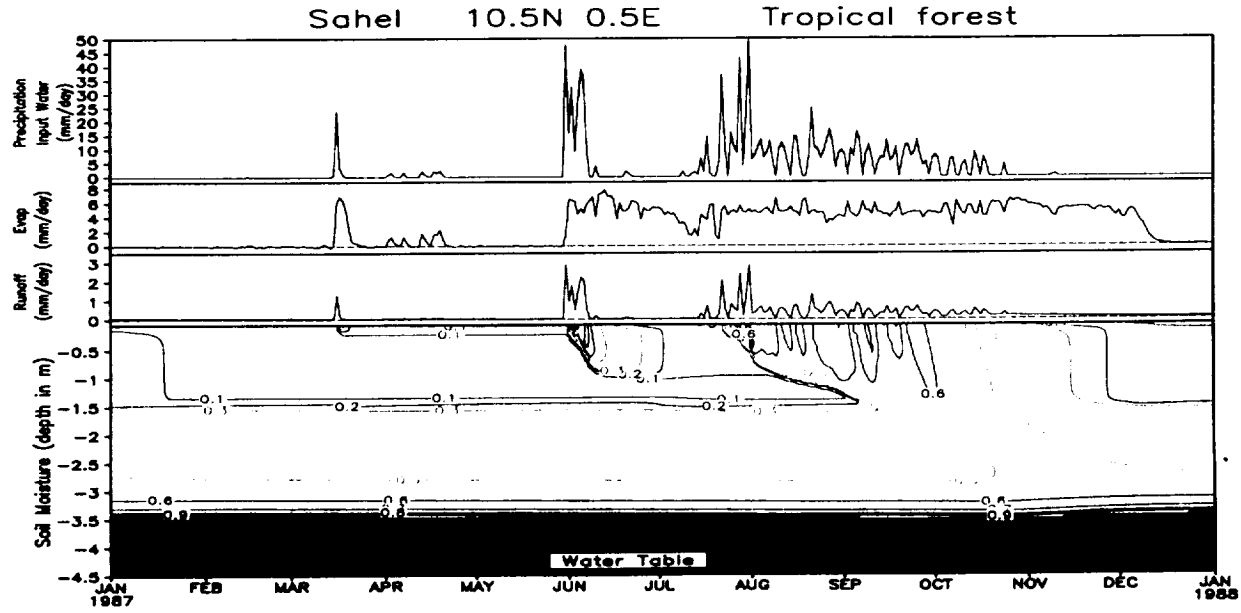
Sahel 10.5N 0.5E Tropical forest
Precipitation Input Water (mm/day)
Evap (mm/day)
Runoff (mm/day)
Soil Moisture (depth in m)
Water Table
JAN 1987
FEB
MAR
APR
MAY
JUN
JUL
AUG
SEP
OCT
NOV
DEC
JAN 1988

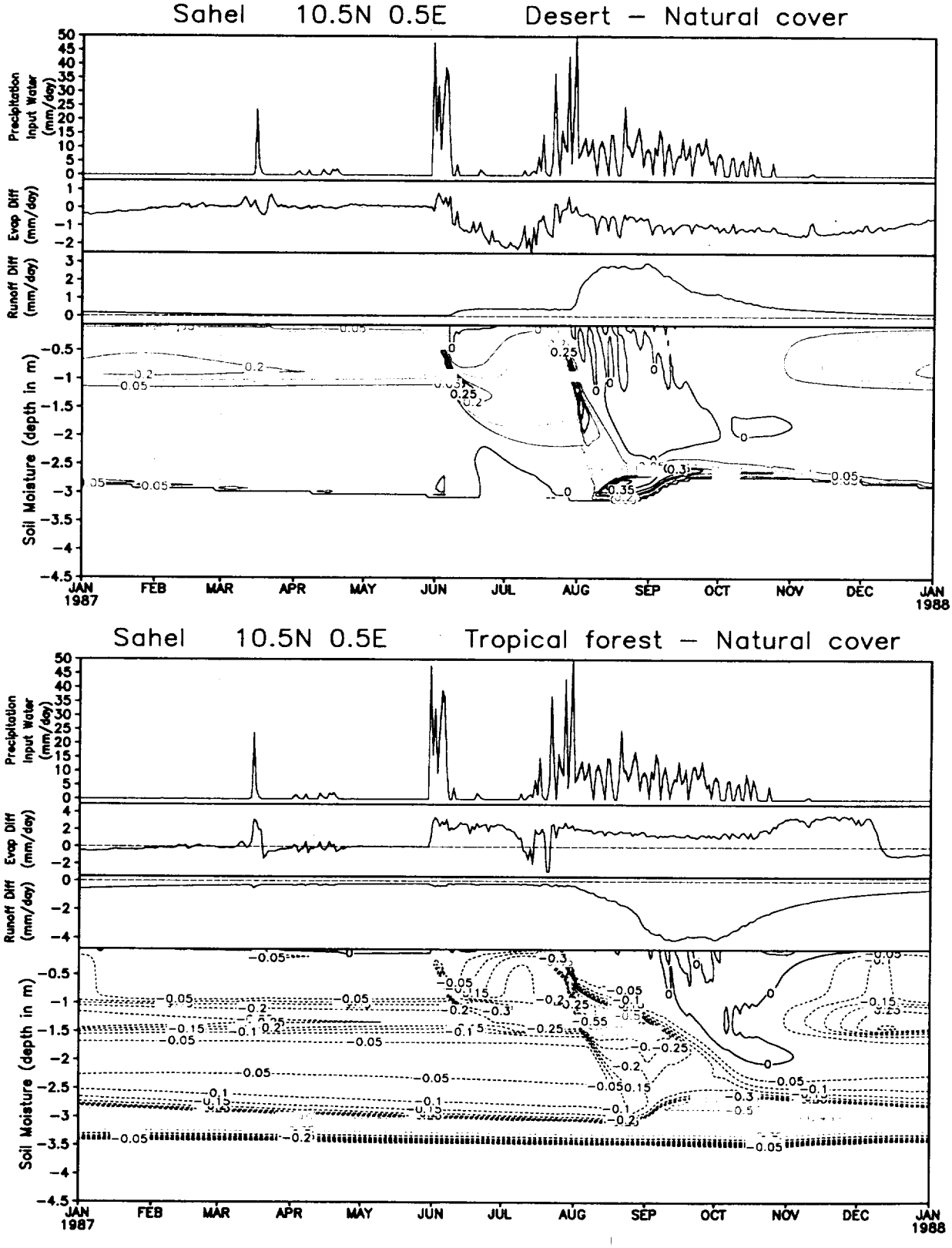
Sahel 10.5N 0.5E Desert – Natural cover
Precipitation Input Water (mm/day)
Evap Diff (mm/day)
Runoff Diff (mm/day)
Soil Moisture (depth in m)
JAN 1987
FEB
MAR
APR
MAY
JUN
JUL
AUG
SEP
OCT
NOV
DEC
JAN 1988
Sahel 10.5N 0.5E Tropical forest – Natural cover
Precipitation Input Water (mm/day)
Evap Diff (mm/day)
Runoff Diff (mm/day)
Soil Moisture (depth in m)
JAN 1987
FEB
MAR
APR
MAY
JUN
JUL
AUG
SEP
OCT
NOV
DEC
JAN 1988

Fig 5b

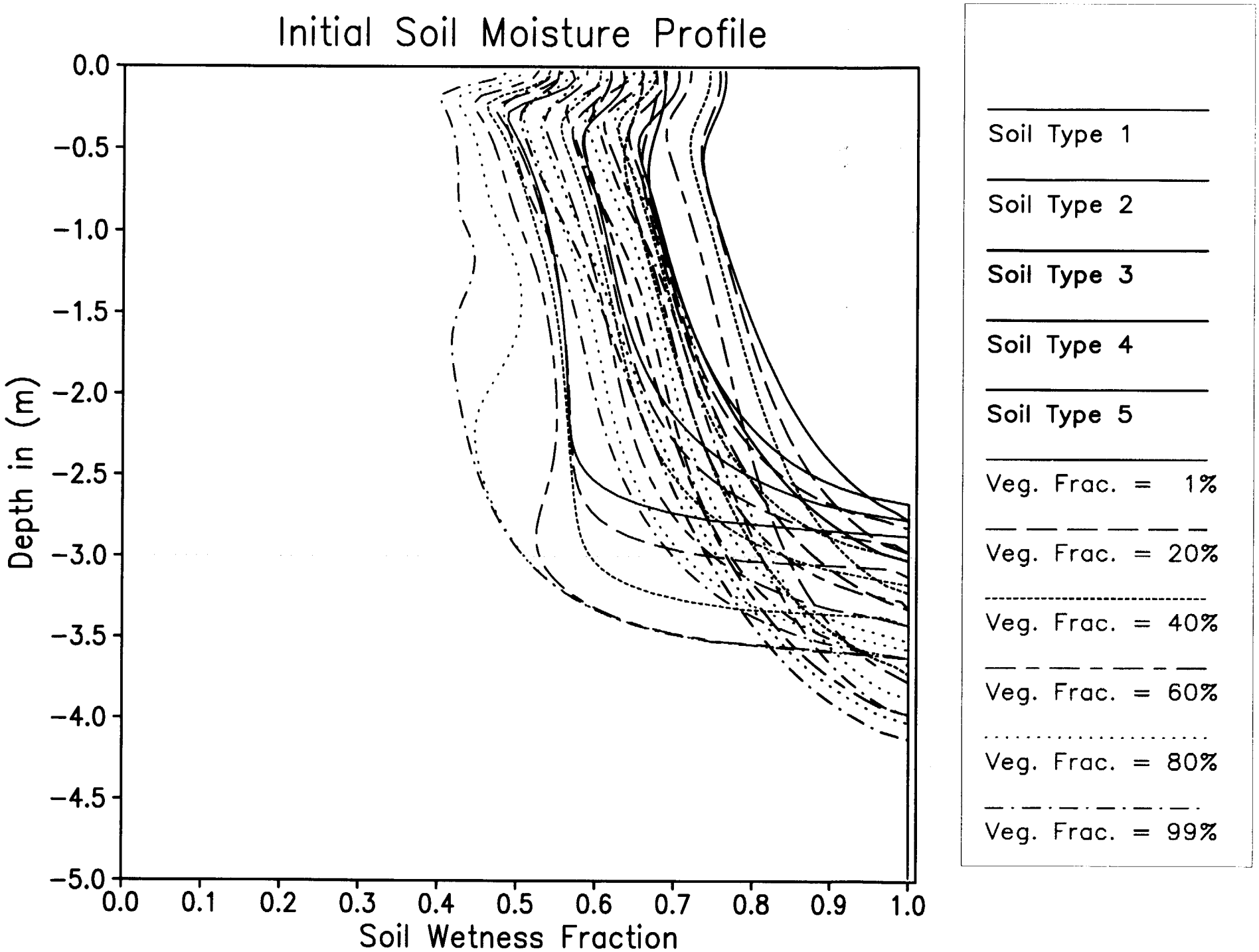
Initial Soil Moisture Profile
Depth in (m)
0.0
-0.5
-1.0
-1.5
-2.0
-2.5
-3.0
-3.5
-4.0
-4.5
-5.0
0.0
0.1
0.2
0.3
0.4
0.5
0.6
0.7
0.8
0.9
1.0
Soil Wetness Fraction
Soil Type 1
Soil Type 2
Soil Type 3
Soil Type 4
Soil Type 5
Veg. Frac. = 1%
Veg. Frac. = 20%
Veg. Frac. = 40%
Veg. Frac. = 60%
Veg. Frac. = 80%
Veg. Frac. = 99%

Fig 7a

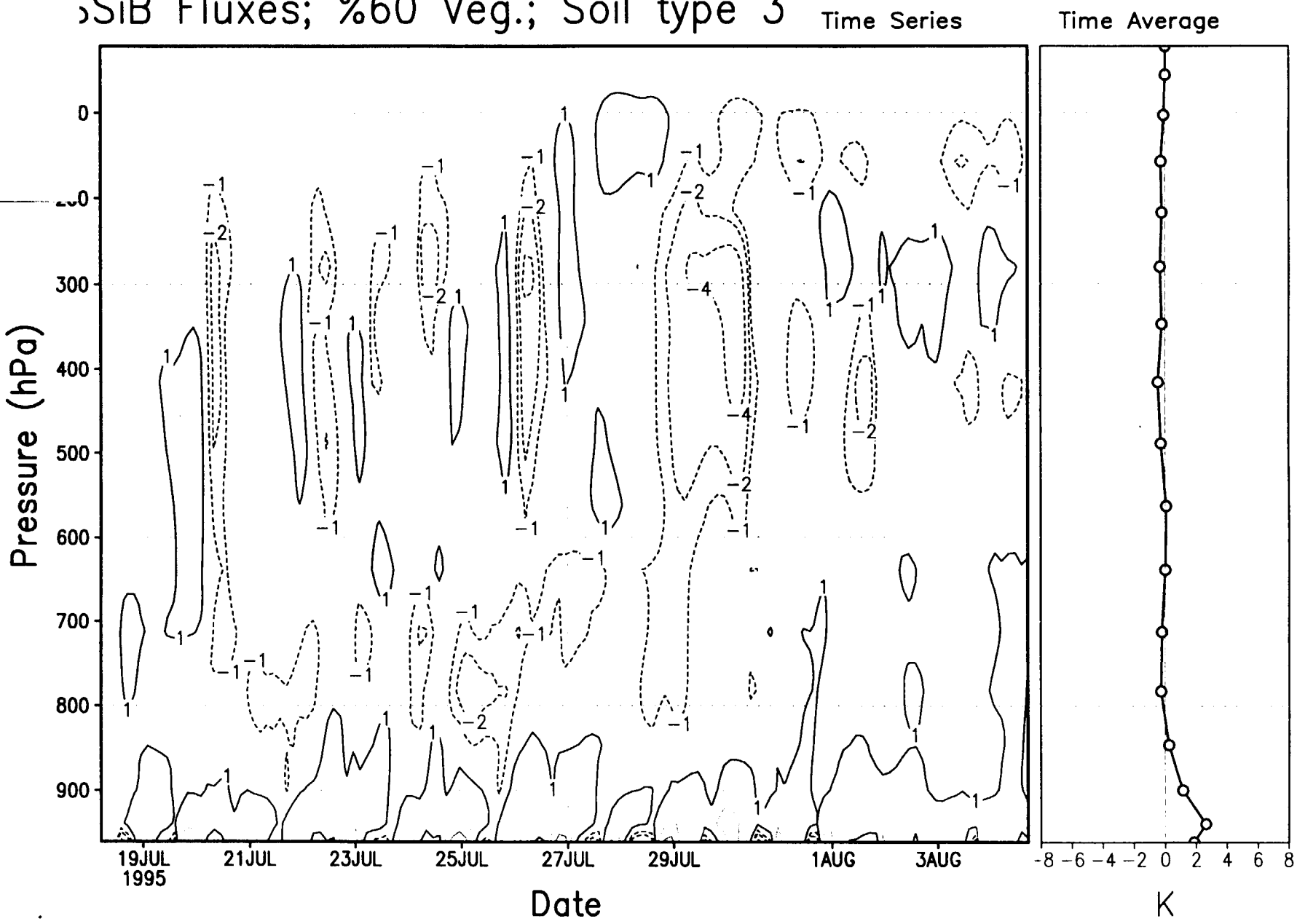

Temperature Error (K) Simulated – ARM Observations.

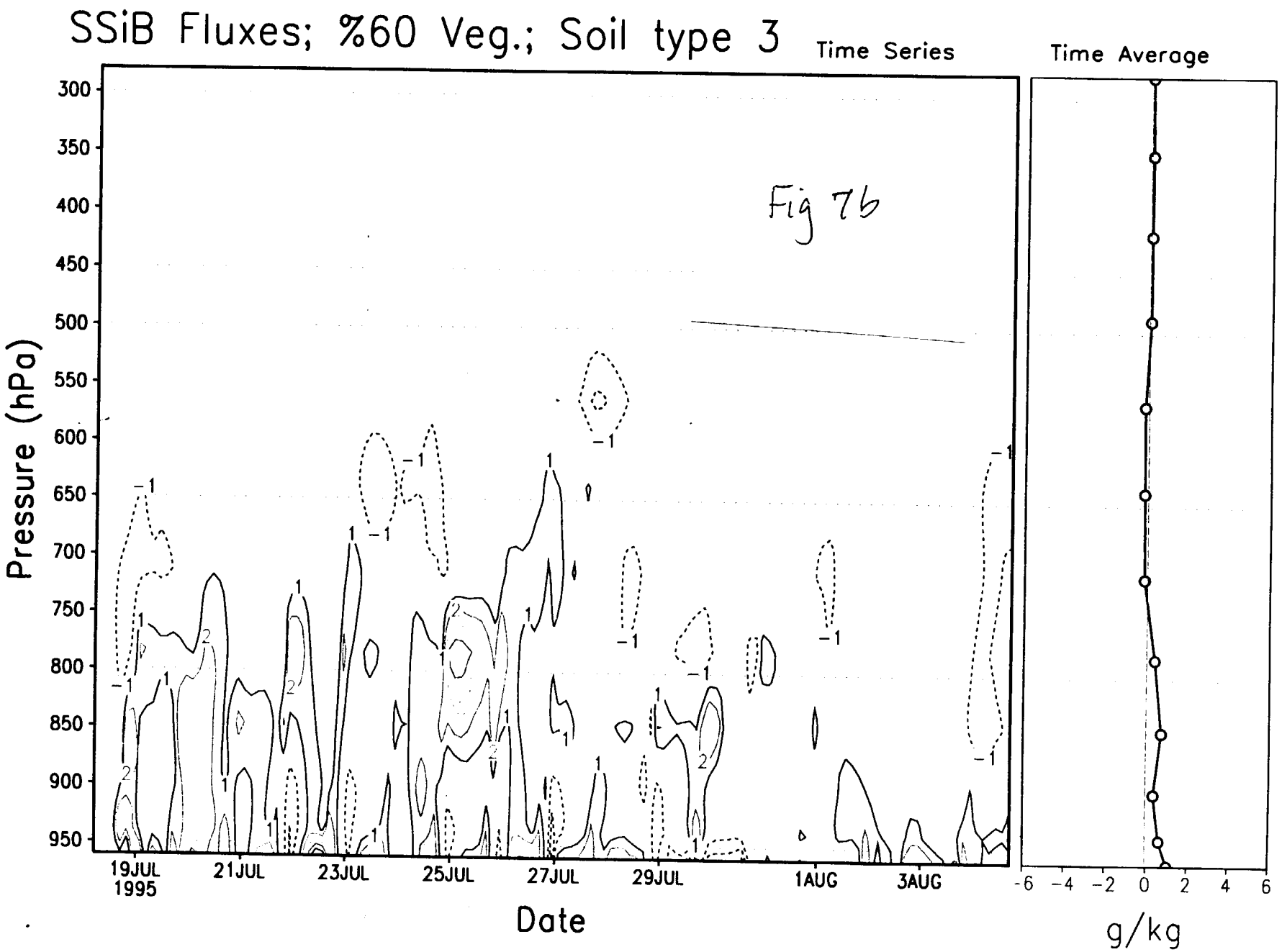

Specific Humidity Error (g/kg) Simulated – ARM Observations.

Fig 7c

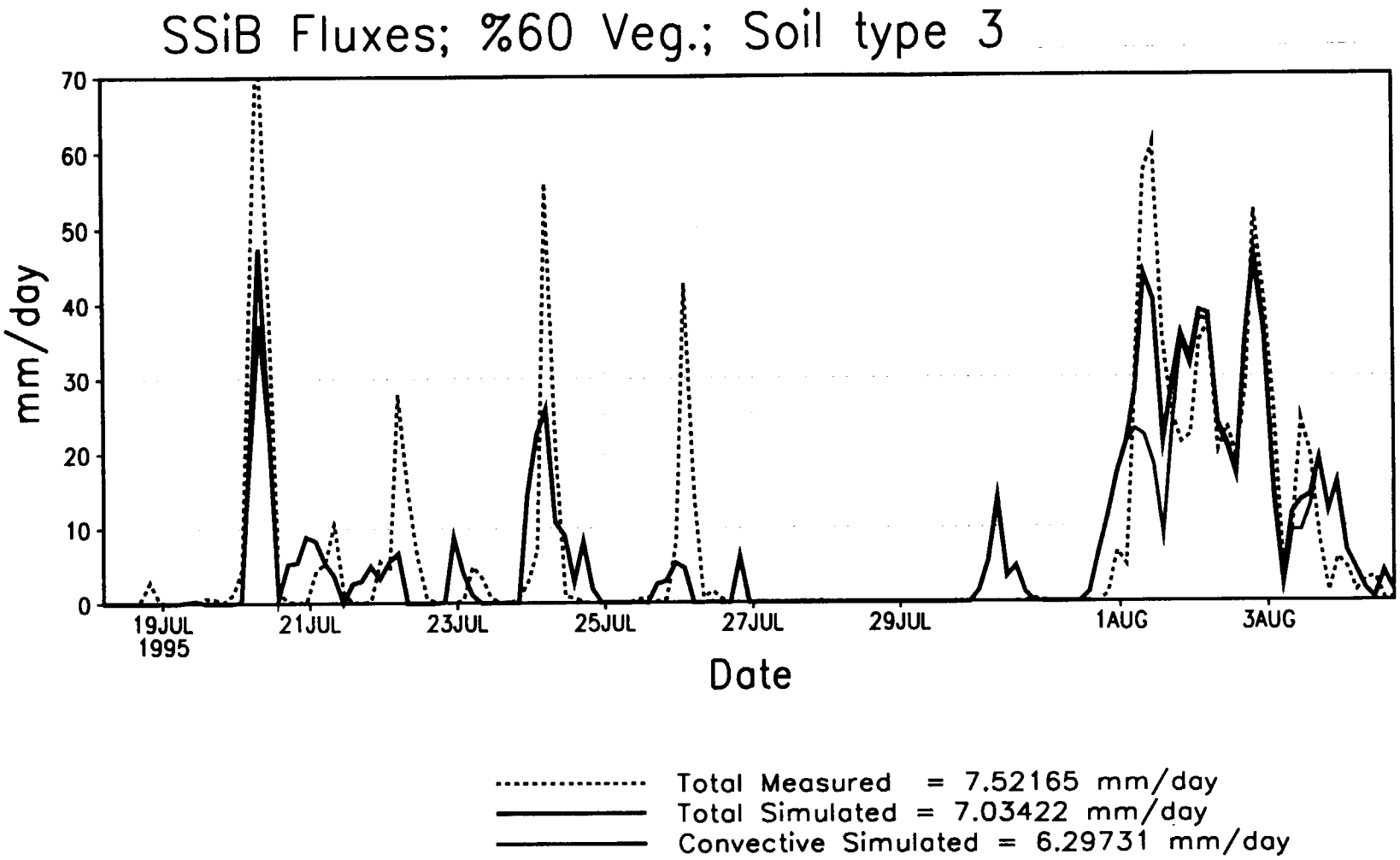
SSiB Fluxes; %60 Veg.; Soil type 3
mm/day
70
60
50
40
30
20
10
0
19JUL
1995
21JUL
23JUL
25JUL
27JUL
29JUL
1AUG
3AUG
Date
Total Measured = 7.52165 mm/day
Total Simulated = 7.03422 mm/day
Convective Simulated = 6.29731 mm/day

Fig 8a

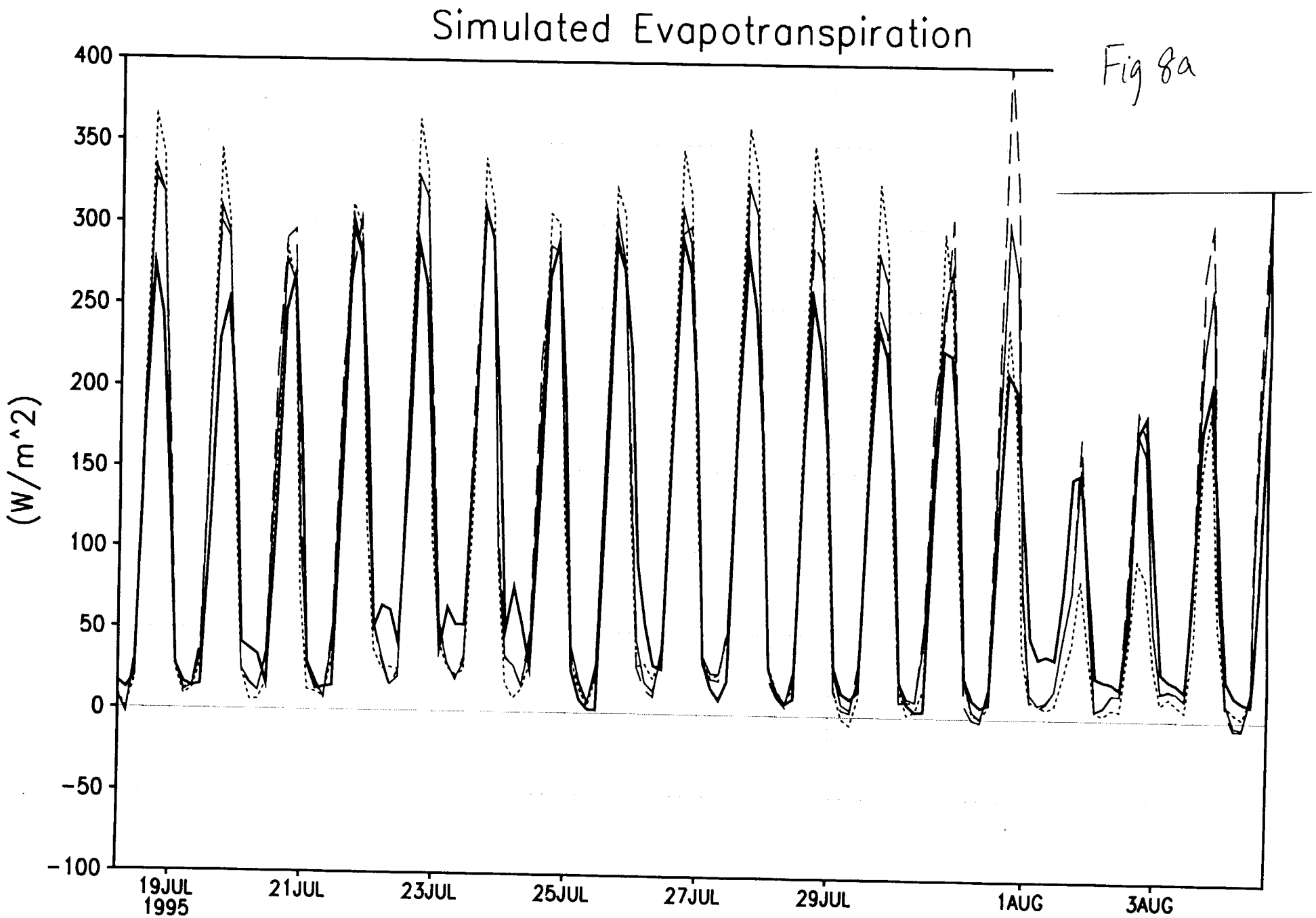

Estimated: Thick
Ave = 109.993

60% Veg.: Thin
Ave = 115.026

99% Veg.: Large Dash
Ave = 118.88

1% Veg.: Small Dash
Ave = 108.983

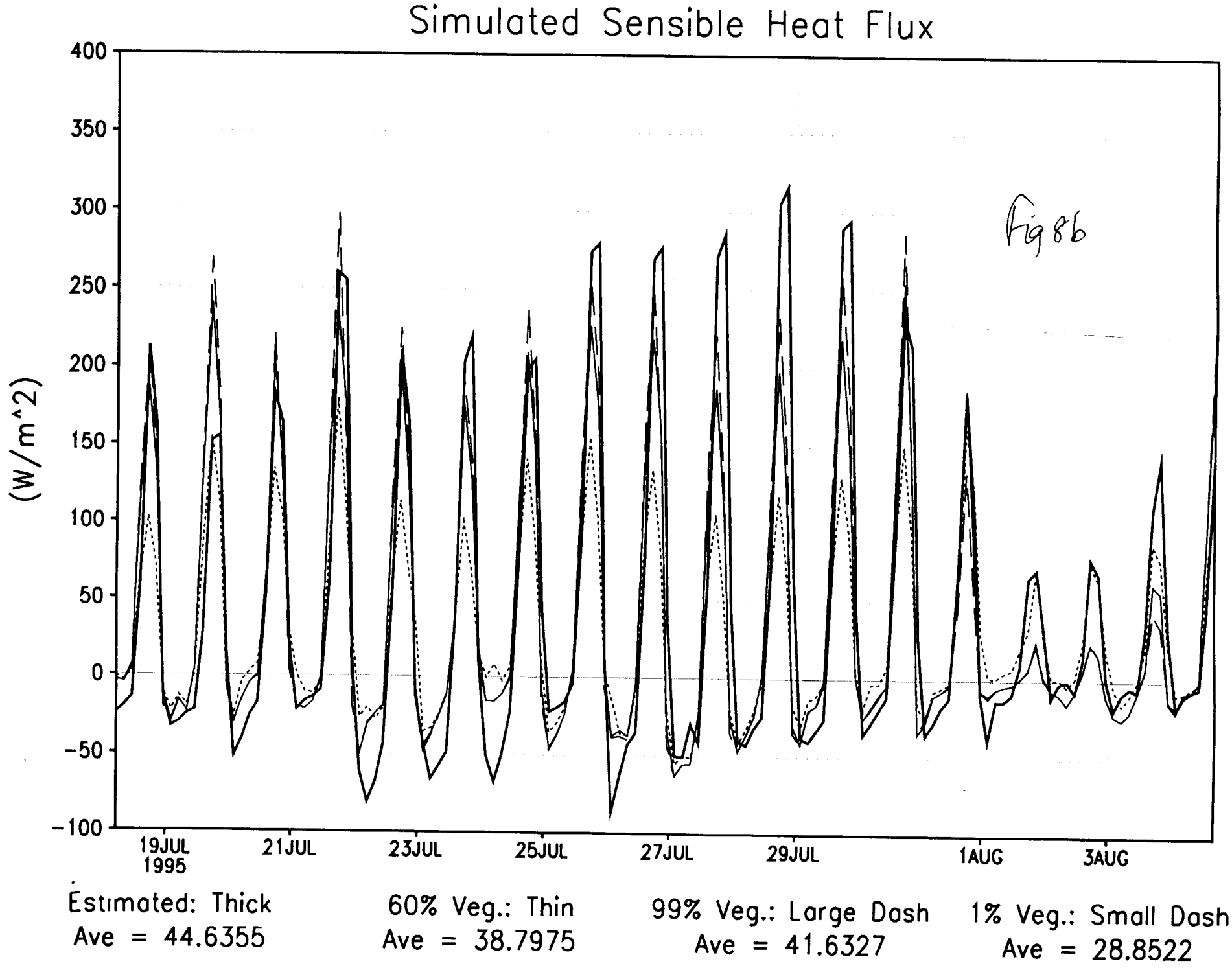
Simulated Sensible Heat Flux
Fig 86
(W/m^2)
400
350
300
250
200
150
100
50
0
-50
-100
19JUL
1995
21JUL
23JUL
25JUL
27JUL
29JUL
1AUG
3AUG
Estimated: Thick
Ave = 44.6355
60% Veg.: Thin
Ave = 38.7975
99% Veg.: Large Dash
Ave = 41.6327
1% Veg.: Small Dash
Ave = 28.8522

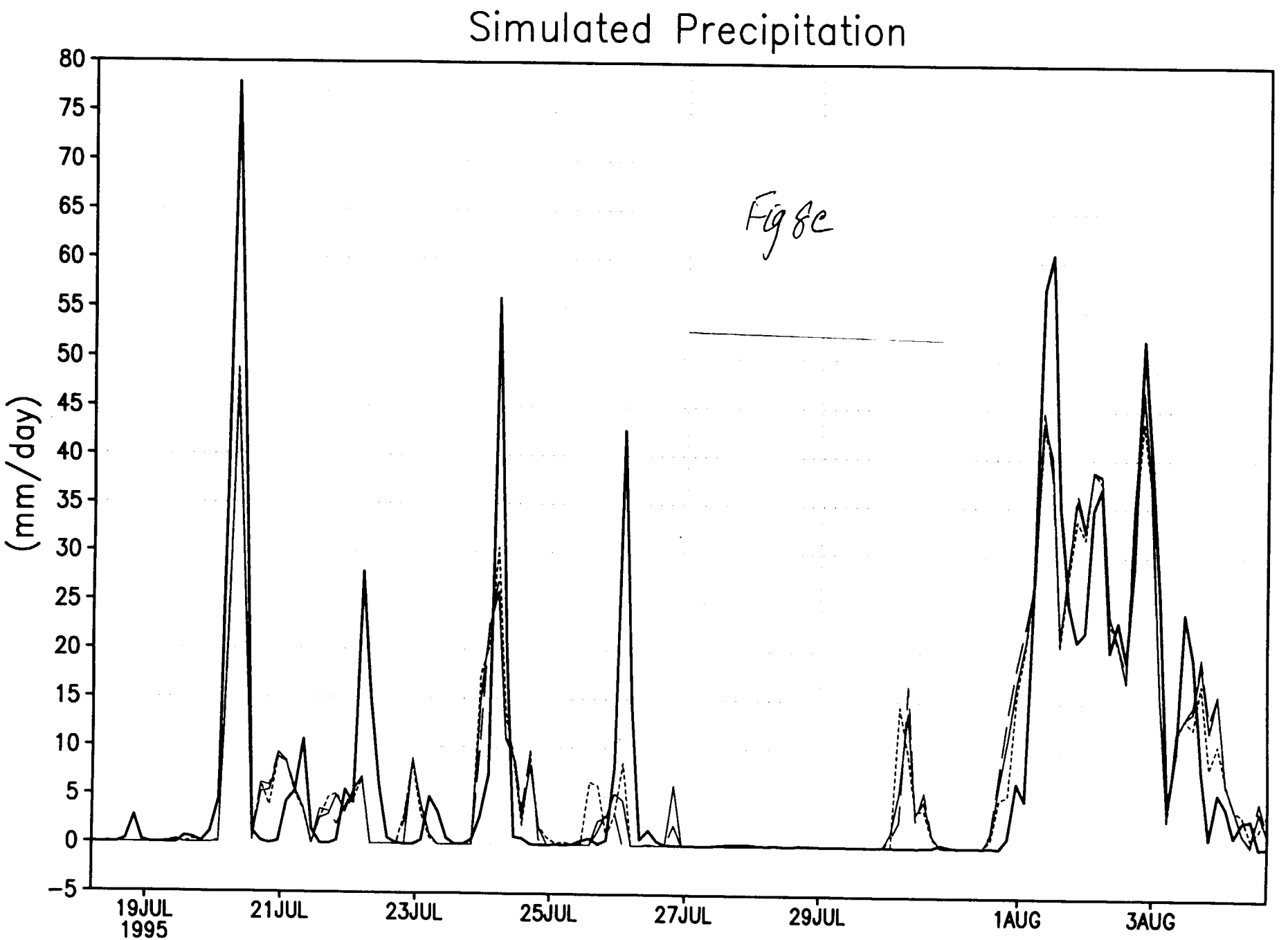
Simulated Precipitation
Fig 8c
(mm/day)
80
75
70
65
60
55
50
45
40
35
30
25
20
15
10
5
0
-5
19JUL
1995
21JUL
23JUL
25JUL
27JUL
29JUL
1AUG
3AUG
Observed: Thick
Ave = 7.52165
60% Veg.: Thin
Ave = 7.03422
99% Veg.: Large Dash
Ave = 7.06112
1% Veg.: Small Dash
Ave = 6.93899

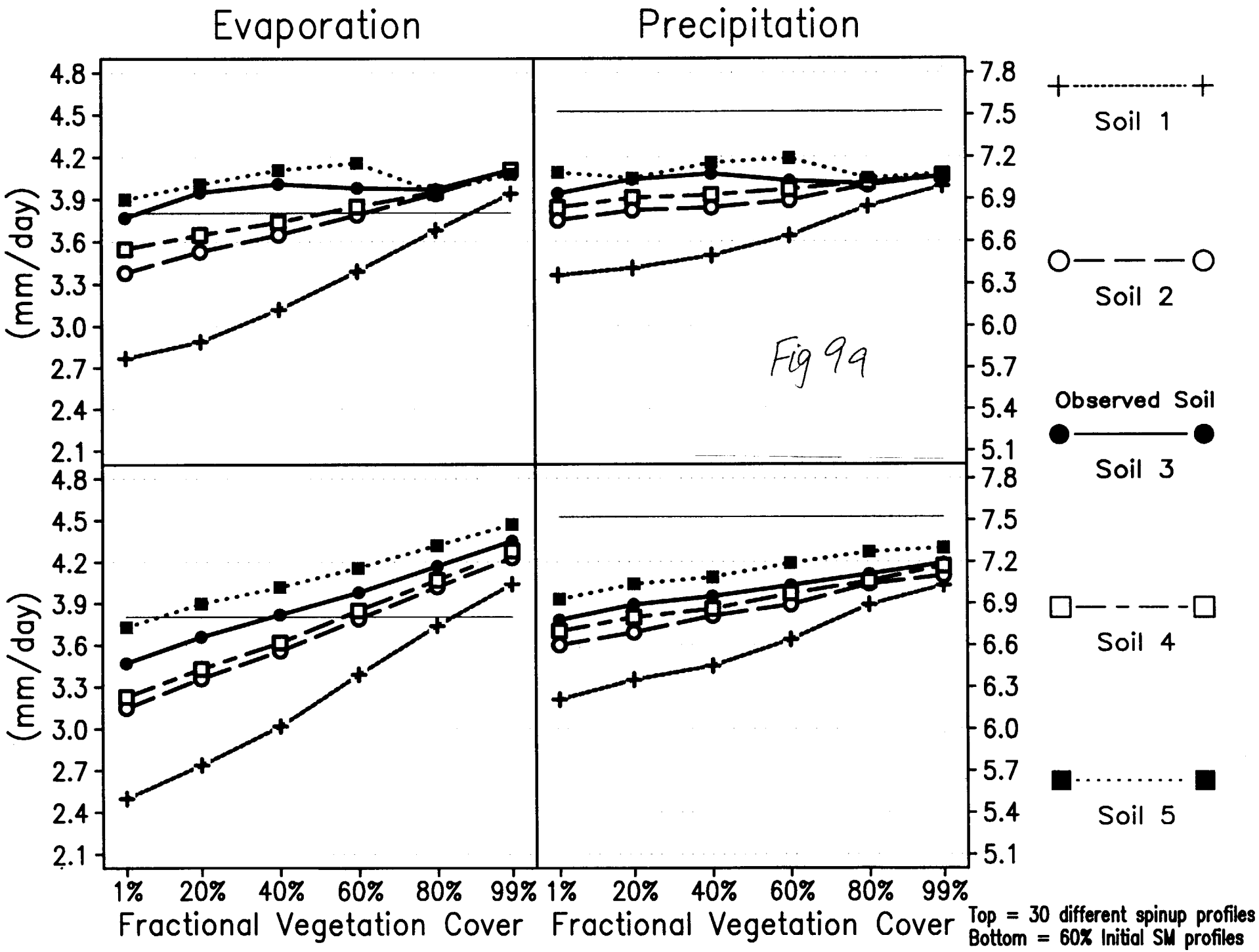
Evaporation
Precipitation
(mm/day)
4.8
4.5
4.2
3.9
3.6
3.3
3.0
2.7
2.4
2.1
7.8
7.5
7.2
6.9
6.6
6.3
6.0
5.7
5.4
5.1
1%
20%
40%
60%
80%
99%
Fractional Vegetation Cover
Soil 1
Soil 2
Observed Soil
Soil 3
Soil 4
Soil 5
Top = 30 different spinup profiles
Bottom = 60% Initial SM profiles

Fig 9a

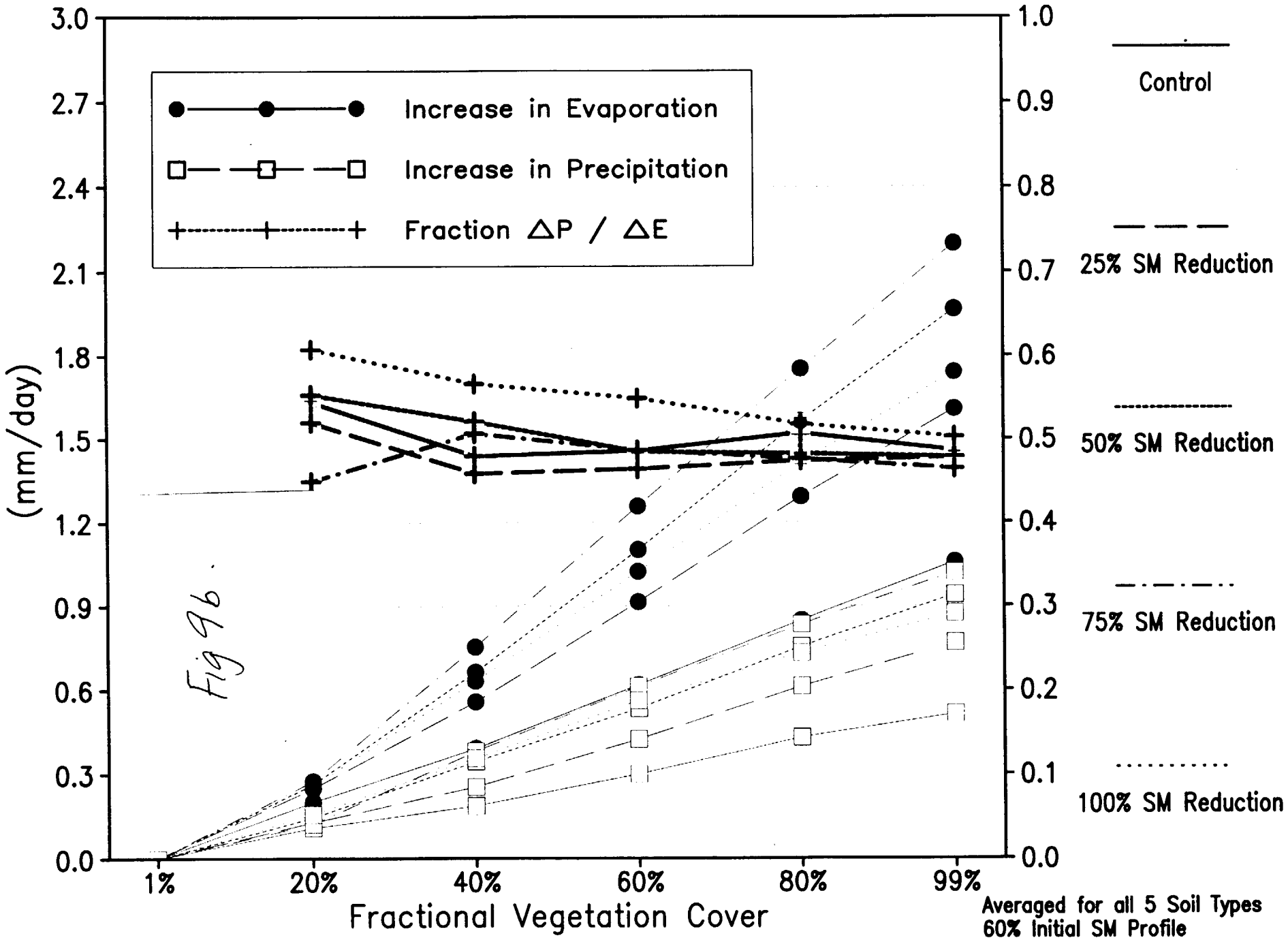
Simulated Increase in Moisture Fields
Increase in Evaporation
Increase in Precipitation
Fraction ΔP / ΔE
(mm/day)
3.0
2.7
2.4
2.1
1.8
1.5
1.2
0.9
0.6
0.3
0.0
1.0
0.9
0.8
0.7
0.6
0.5
0.4
0.3
0.2
0.1
0.0
1%
20%
40%
60%
80%
99%
Fractional Vegetation Cover
Control
25% SM Reduction
50% SM Reduction
75% SM Reduction
100% SM Reduction
Averaged for all 5 Soil Types
60% Initial SM Profile
Fig 96.

Fig 9c

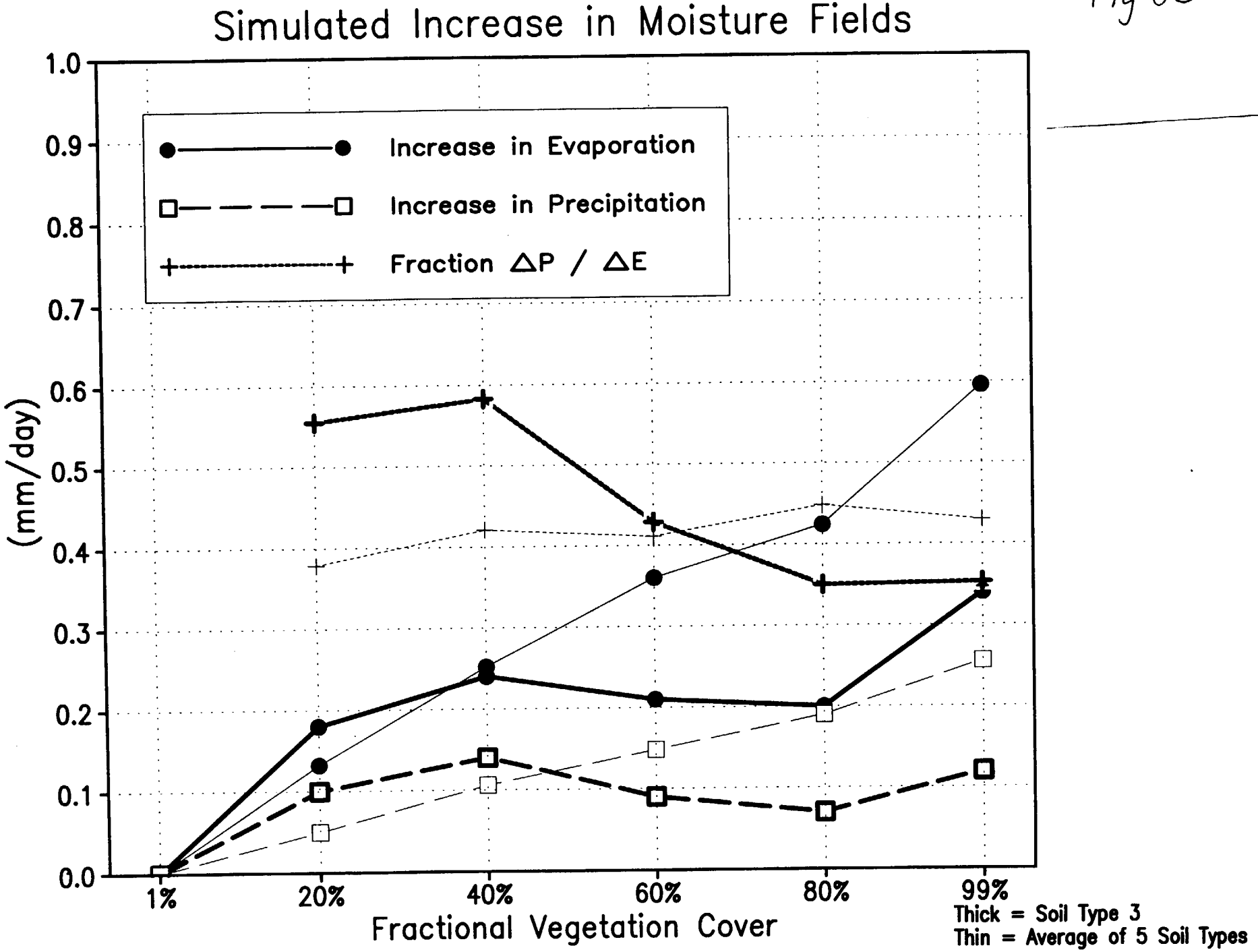
Simulated Increase in Moisture Fields
Increase in Evaporation
Increase in Precipitation
Fraction ΔP / ΔE
(mm/day)
1.0
0.9
0.8
0.7
0.6
0.5
0.4
0.3
0.2
0.1
0.0
1%
20%
40%
60%
80%
99%
Fractional Vegetation Cover
Thick = Soil Type 3
Thin = Average of 5 Soil Types

Fig 10a

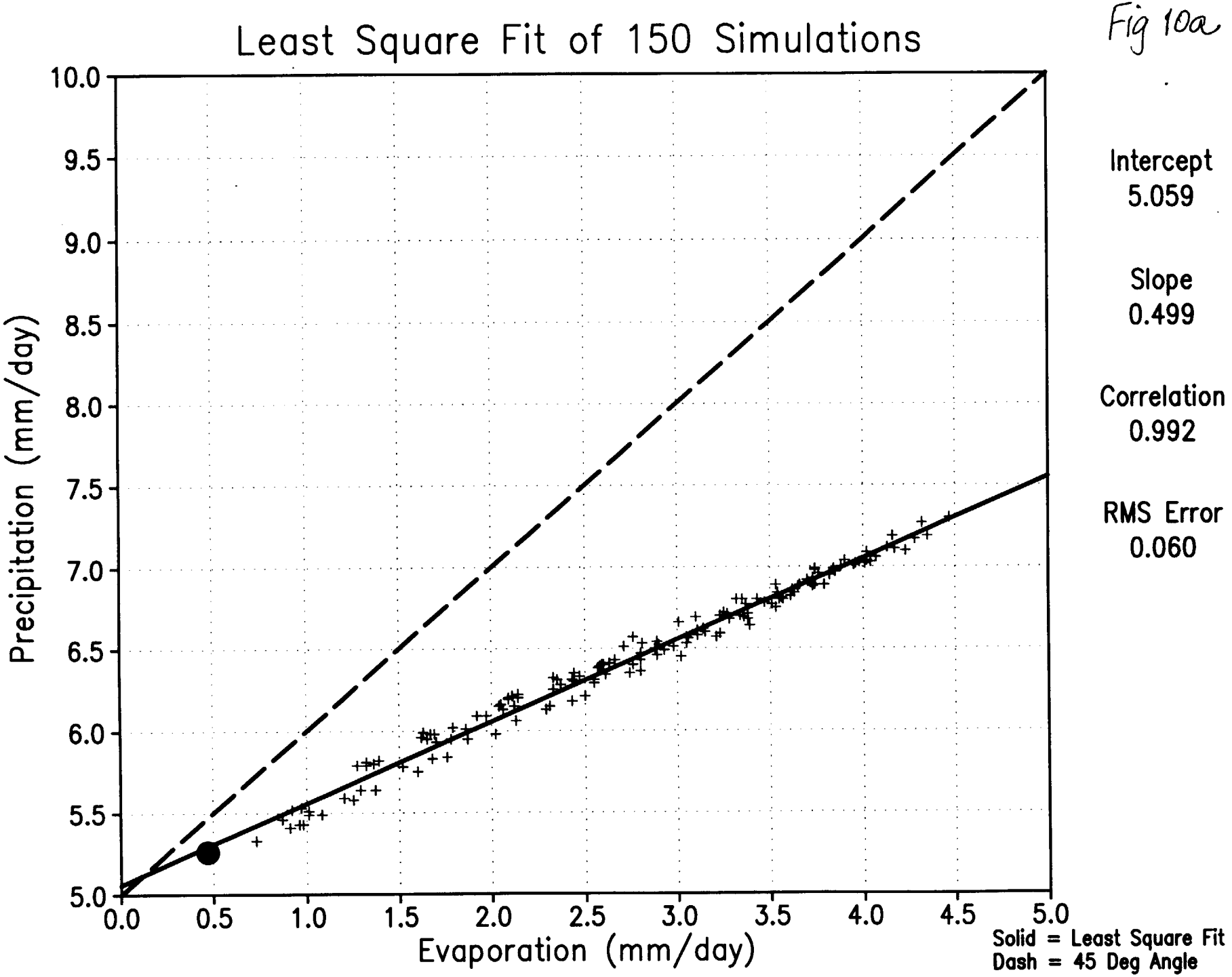
Least Square Fit of 150 Simulations
Precipitation (mm/day)
Evaporation (mm/day)
10.0
9.5
9.0
8.5
8.0
7.5
7.0
6.5
6.0
5.5
5.0
0.0
0.5
1.0
1.5
2.0
2.5
3.0
3.5
4.0
4.5
5.0
Intercept
5.059
Slope
0.499
Correlation
0.992
RMS Error
0.060
Solid = Least Square Fit
Dash = 45 Deg Angle

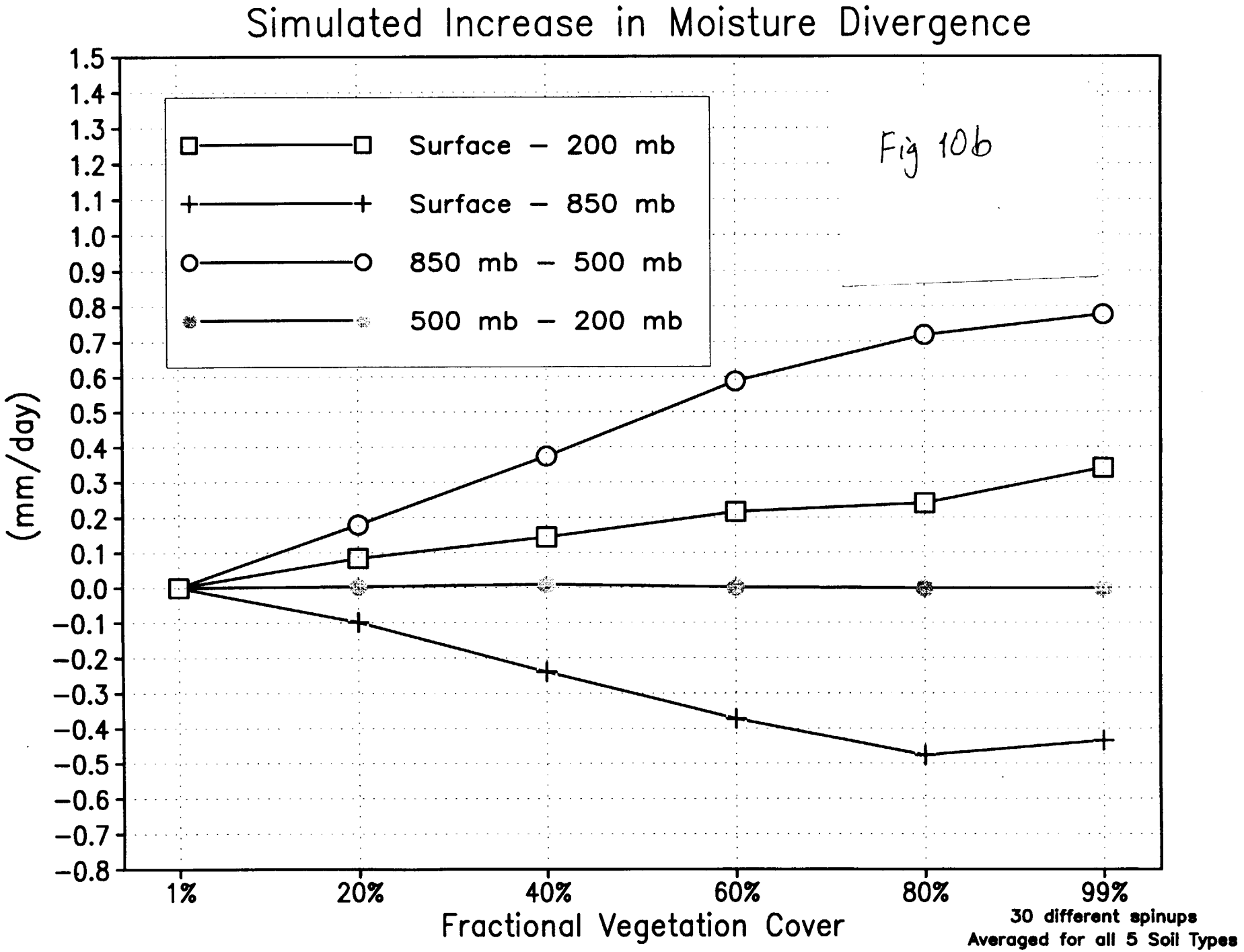
Simulated Increase in Moisture Divergence
Fig 10b
Surface – 200 mb
Surface – 850 mb
850 mb – 500 mb
500 mb – 200 mb
(mm/day)
1.5
1.4
1.3
1.2
1.1
1.0
0.9
0.8
0.7
0.6
0.5
0.4
0.3
0.2
0.1
0.0
−0.1
−0.2
−0.3
−0.4
−0.5
−0.6
−0.7
−0.8
1%
20%
40%
60%
80%
99%
Fractional Vegetation Cover
30 different spinups
Averaged for all 5 Soil Types

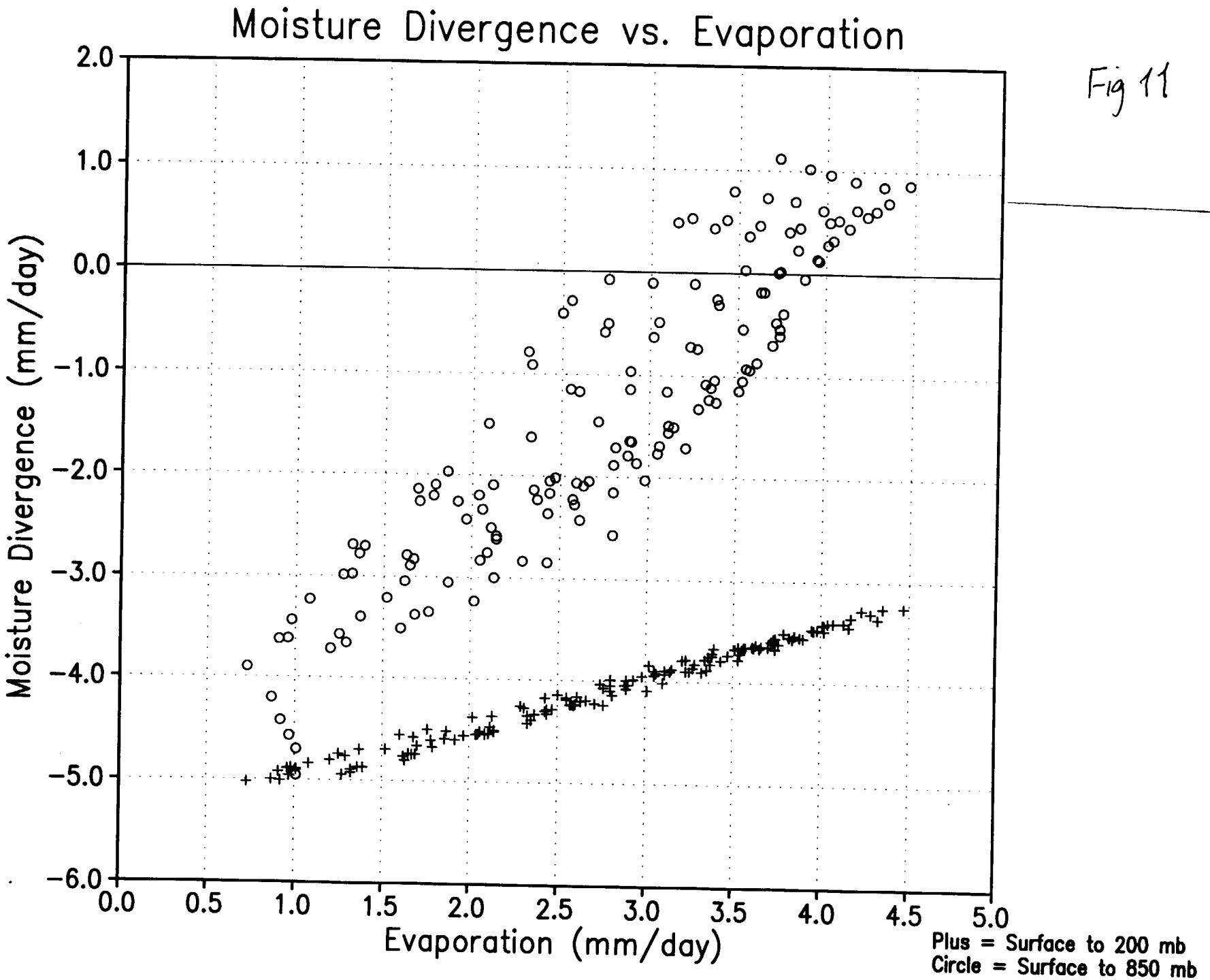
Moisture Divergence vs. Evaporation
Moisture Divergence (mm/day)
2.0
1.0
0.0
-1.0
-2.0
-3.0
-4.0
-5.0
-6.0
0.0
0.5
1.0
1.5
2.0
2.5
3.0
3.5
4.0
4.5
5.0
Evaporation (mm/day)
Plus = Surface to 200 mb
Circle = Surface to 850 mb

Fig 11